The Thesis Committee for Patricia Bo Cho
certifies that this is the approved version of the following thesis:

Simulation of Stark Broadened Hydrogen Balmer Line Shapes for DA White Dwarf Synthetic Spectra

SUPERVISING COMMITTEE:

Don Winget, Supervisor

Mike Montgomery, Co-Supervisor

Volker Bromm

Thomas Gomez

Keith Hawkins

Chris Sneden

Simulation of Stark Broadened Hydrogen Balmer Line Shapes for DA White Dwarf Synthetic Spectra

by

Patricia Bo Cho

THESIS

Presented to the Faculty of the Graduate School of

The University of Texas at Austin

in Partial Fulfillment

of the Requirements

for the Degree of

MASTER OF ARTS

THE UNIVERSITY OF TEXAS AT AUSTIN

May 2021

Dedicated to Toru Okada, without whom we might all have been lost.

Acknowledgments

I would like to thank my advisors Don Winget and Mike Montgomery for their support and generosity, for letting me tag along to witness my first set of shots, for leaving all of the doors open, and for opening a few more for me along the way. I would especially like to thank Thomas Gomez for gifting me with Xenomorph, for his invaluable help and advice, and for his endless patience. Without him, this thesis would not exist. I offer my gratitude to Haruki Murakami, Min Jin Lee, Octavia Butler, Ocean Vuong, Elif Batuman, and Kazuo Ishiguro for building worlds I could wrap around myself during the dimmer times.

Simulation of Stark Broadened Hydrogen Balmer Line Shapes for DA White Dwarf Synthetic Spectra

Patricia Bo Cho, M.A.
The University of Texas at Austin, 2021

Supervisors: Don Winget
Mike Montgomery

White Dwarfs (WD) are useful across a surprisingly wide range of astrophysical contexts from cosmochronology to piecing together the chemical enrichment history of a galaxy throughout the cycles of star formation to their use as spectrophotometric standards for many major astronomical observatories. In all of these contexts, the fidelity of the information we can extract is predicated on the accuracy of our model atmosphere calculations. Interpretations of actual WD stellar spectral and photometric data depend in one way or another on fits to grids of model atmospheres. The codes used to construct these grids have relied on the basic model of Vidal et al. (1970) (VCS), known as the Unified Theory of line broadening for line shape calculations. There have since been significant advancements in the theory, however, the calculations used in WD model atmospheres have only received

minor updates. Meanwhile, continued advances in spectroscopic instrumentation and signal-to-noise of stellar spectral data have uncovered indications of inaccuracies in the VCS theory. The improvements in the fidelity of our data have signaled a simultaneous decline in the fidelity of our spectral fits and fundamental parameter determinations. The inaccuracies manifest as discrepancies in mean mass estimates made using different mass determination techniques. Additionally, fits performed using individual spectral lines as opposed to the entire set of lines Hβ-H8 also yield highly discrepant inferred values for mass and temperature. Motivated by this, Gomez et al. (2016) developed a simulation based line profile calculation code *Xenomorph* using an improved theoretical treatment of Stark Broadened line profiles themselves. This code made the theoretical line shape advancements available to the WD community for the first time. However, the code required a series of revisions to make it more physically realistic as well as to the numerical methods to make the calculations computationally tractable for the large grids needed for model atmosphere calculations. Comparisons against the standard Tremblay & Bergeron (2009) line shape calculations also demanded an implementation of a simulation based approach to occupation probability. This thesis presents a detailed description of these changes which now make full grids of new and improved line profile calculations feasible and appropriate for use in WD model atmosphere calculations.

Table of Contents

Acknowledgments **v**

Abstract **vi**

List of Figures **x**

Chapter 1. Overview **1**

Chapter 2. Simulation Stark Broadened Hydrogen Balmer Line Shapes[1] **10**

2.1 Line Broadening in WD Atmospheres 10

2.2 Simulation 15

2.2.1 Plasma Construction and Numerics 15

2.2.2 Randomness: Impact Parameter and Maxwellian Velocity Distributions 17

2.2.3 Additional Considerations: Microfield Distribution and Poisson Statistics 20

2.2.4 Debye Screening Effects 22

2.2.5 Choice of Numerical Method: Autocorrelation vs. Power Spectrum 26

2.2.6 VCS Shortcomings 29

2.3 New Physics 31

2.3.1 Agreement with Previous Theory 31

2.3.2 Ion Dynamics 34

2.3.3 Multipole Expansion 34

2.3.4 Expanded Basis Set 38

2.3.5 Occupation Probability 38

2.4 Comparison to Experiment 43

2.5 Summary 51

Chapter 3. Outlook **55**

Bibliography **58**

Vita **62**

List of Figures

1.1 This figure is a reproduction of Fig. 6 from (Fontaine et al., 2001). Each line is a calculation for the luminosity function of the population of WDs assuming a different age for the Galactic disk. For different ages of the Galaxy, the number of WDs in each luminosity bin does not vary on the ascending branches but there is a very clear divergence shortly after the peak. As the galaxy ages, more of the WD population has had more time to cool and the numbers of white dwarfs in the lower luminosity bins gradually increase. Measuring the luminosities of a population of white dwarfs and fitting them with a set of theoretical luminosity functions such as the ones in this plot allow us to place a constraint on the age of the galaxy or cluster they live in. 2

2.1 Typical DA white dwarf atmospheric structure. Temperature and density profiles are shown as a function of optical depth for a model with $T_{\rm eff}$ = 20,000K and log g = 8. The blue shaded region corresponds to the parameter space covered by the VCS line profiles calculated by Lemke and used to calculate opacities for bound-bound Hydrogen transitions. The vertical dotted lines show conditions at three different optical depths and the horizontal dashed lines point to the conditions at an optical depth of $\tau = 2/3$. The grey shaded region demonstrates the typical range of experimental conditions achievable on the Z-machine. Two different atmosphere models were constructed: one with the VCS line shapes and another with the new Xenomorph profiles containing all of the new features. This ensures the maximum amount of difference between the profiles. The atmospheric structure remains unchanged. The largest difference observed between the two models is less than a percent in the temperature at an optical depth of 10. Therefore, the differences in the profiles are not significant enough to induce a change in the temperature and density profiles of the atmospheres. 11

2.2 Density at depth of formation point for three DA atmosphere models with $T_{\rm eff} = 15,000K$ and $T_{\rm eff} = 20,000K$ for three different values of log g. 13

2.3 Temperature at depth of formation point on extended wavelength range for three DA atmosphere models with $T_{\rm eff} = 15,000K$ and $T_{\rm eff} = 20,000K$ for three different values of log g. The Balmer region of the spectrum is formed higher and at cooler temperatures than the stellar effective temperature. 14

2.4 Impact parameter and velocity distributions. Both distribution curves are properly preserved when their probability distribution functions are modified by the lifetime for reinjected particles. 21

2.5 Comparisons of microfield distributions. The Hooper microfield distribution is still properly recovered by the new re-injection scheme. Therefore, we can be confident that the new reinjection scheme is properly implemented with regard to its ability to generate the proper microfield distribution. 23

2.6 The effect of screening on line shape FWHM for Hβ. Increasing the amount of screening experienced by the plasma particles yields narrower lines. Doubly screening ions (in other words, screening ions by both ions and electrons) produces a narrower profile (smaller FWHM) than singly screening both types of particles. 27

2.7 Representative Hβ line shape on a linear scale (top) and log scale (bottom). The noise properties of the power spectrum method yield line shapes that are clean enough to use in model atmospheres. 32

2.8 Hα calculations with new physics features turned on. Where labeled, each profile includes only one of the additional pieces of input physics. For example, the calculations labeled "Xeno: idyn" use static ions but does not include higher order multipole terms in the Coulomb potential or an expanded basis set. However, all other profiles have been calculated with ion dynamics turned on. For example, the calculations labeled "Xeno: quad" use both static ions and expand the Coulomb interaction potential to include the quadrupole moment but does not use an expanded basis set. This choice follows from the fact that the prolonged presence of a close ion throughout the duration of a given iteration generates large artificial deposits of power in the line profile. This occurs at the frequency corresponding to the disproportionately large and persistent Efield generated by the close ion. Static ions therefore generate spiky profiles in the far wings due to these close ion approaches, and we leave ion dynamics on to avoid this type of pathological behavior in the simulation and in the profiles. Comparisons between VCS and *Xenomorph* exhibit expected disagreement in the height of the cores of the profiles. Inclusion of time ordering in the *Xenomorph* calculations depresses peak height which increases the FWHM. The wings show good agreement between the two theories. 35

2.9 Hβ calculations with new physics features turned on. The inclusion of time ordering yields the expected result of decrased relative intensity in the core central dip of the profiles. The wings again show good agreement between the two theories. . 36

2.10 Hγ calculations with new physics features turned on. The effects of time ordering are again evident as in the Hα and Hβ calculations, and again we see excellent agreement in the wings of the profiles. 37

2.11 Comparison of full line shapes with exponentially damped electron broadening profiles. We apply the wing damping described in TB09 to the VCS profiles as well as to *Xenomorph* calculations performed with the HM88 occupation probability prescription. We achieve decent correspondence TB09 out to about 1 eV if we decrease the rest transition energy in the exponential term by a factor of 2. 43

2.12 Ion and electron microfield distributions compared to Hooper. The ion microfield distribution changes in response to the occupation probability prescription used. Limiting the closest approach of plasma ions and electrons skews the distribution toward smaller electric field values as expected. The vertical dotted line corresponds to the $\beta_{\rm crit}$ value referenced in TB09 — the critical microfield cutoff value. There is very good correspondence between the cutoff in the microfield distribution produced by the HM88 implementation of occupation probability and $\beta_{\rm crit}$. 44

2.13 Line shape comparison with different occupation probability prescriptions. Incorporating occupation probability results in narrower line shapes. FM02 uses a more severe microfield cutoff compared to HM88. The lower electric field values corresponding to FM02 allows only smaller perturbations and therefore leads to narrower line cores. The wings of the line profiles calculated with FM02 and HM88 are almost identical. 45

2.14 Hα calculations comparing different microfield prescriptions. . 46

2.15 Hβ calculations comparing different microfield prescriptions. . 47

2.16 Hγ calculations comparing different microfield prescriptions. The effects of time ordering are again evident as in the Hα and Hβ calculations, and again we see excellent agreement in the wings of the profiles. 48

2.17 Fits to high density Wiese data: Hβ. The core asymmetry is much more accurately predicted by Xenomorph which significantly improves chi-square. 50

2.18 Fits to high density Wiese data: Hγ. The best fit number density obtained using *Xenomorph* is almost identical to that obtained for Hβ. On the other hand, the number density obtained using fits to TB09 profiles are roughly 12% higher than that obtained for Hβ. 51

Chapter 1

Overview

White Dwarfs (WD) represent the end stage of the vast majority of stars (97%) in our universe (Van Horn, 2015). Their intrinsic properties and ubiquity make them useful in a surprisingly wide range of astrophysical contexts. One of the most well known and historically well established of these is cosmochronology (Winget et al., 1987; Fontaine et al., 2001). The WD luminosity function is governed by a set of well constrained theoretical curves. Each of the curves corresponds to the theoretically expected luminosity function for a population of WDs given the age of the overall group that they belong to. The shape of the curves does not vary with age on the ascending branch, but after a certain upper limit, it begins to exhibit a very strong dependence on age at lower luminosities. Fitting the luminosity function of a population of white dwarfs sets a constraint on the age of the galaxy or cluster that they belong to. We can therefore use WDs to determine cosmic ages of various celestial bodies including our own Galaxy which in turn places constraints on the total age of the universe.

Another very different setting where WDs turn out to be useful is in the context of cycles of star formation. Measuring the initial-final mass relation

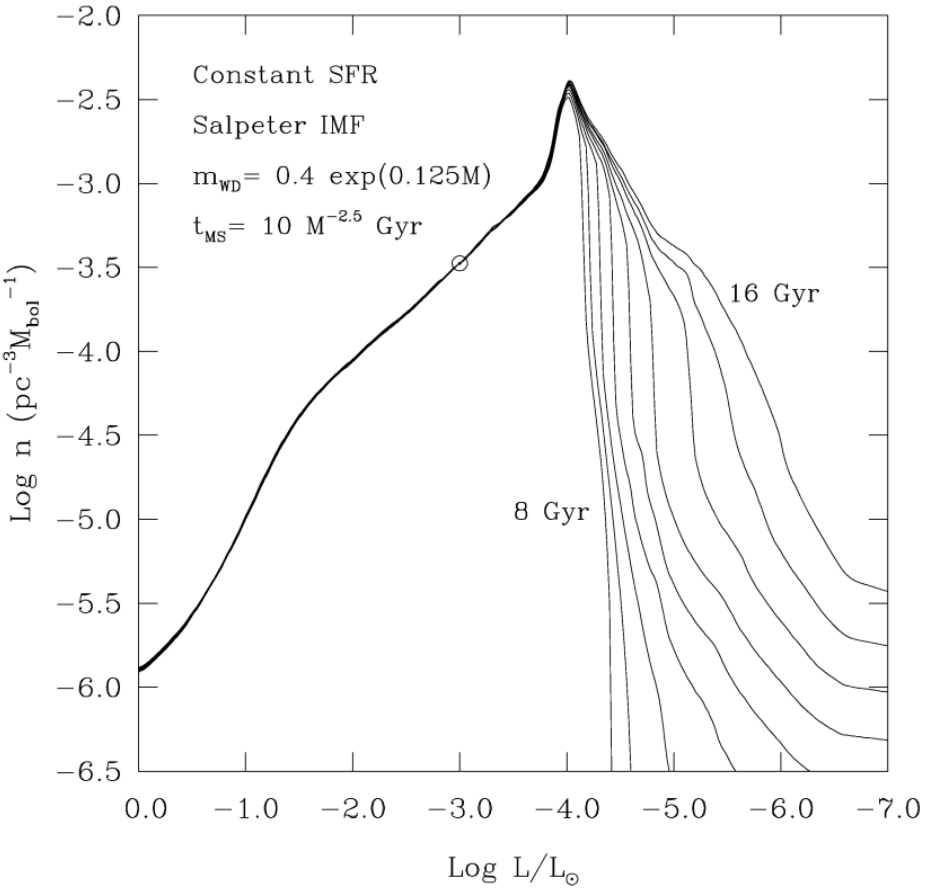

Figure 1.1: This figure is a reproduction of Fig. 6 from (Fontaine et al., 2001). Each line is a calculation for the luminosity function of the population of WDs assuming a different age for the Galactic disk. For different ages of the Galaxy, the number of WDs in each luminosity bin does not vary on the ascending branches but there is a very clear divergence shortly after the peak. As the galaxy ages, more of the WD population has had more time to cool and the numbers of white dwarfs in the lower luminosity bins gradually increase. Measuring the luminosities of a population of white dwarfs and fitting them with a set of theoretical luminosity functions such as the ones in this plot allow us to place a constraint on the age of the galaxy or cluster they live in.

can help us quantify mass loss throughout stellar evolution and provides information about chemical enrichment of subsequent stellar generations (Marigo, 2001). Perhaps the most widely relevant application which holds relevance for the general astronomical community as a whole is the fact that hot WDs are used as spectrophotometric standards for many major observatories and instruments including Hubble, SDSS, ESO, and Kitt Peak (Narayan et al., 2019). In all of these contexts, the fidelity of the information we can extract is predicated on the accuracy of our model atmosphere calculations.

Our inferences rely on determinations of the fundamental stellar properties of effective temperature and surface gravity. The key to determining these quantities is through plasma properties. In the case of DA WDs, the relevant plasma is the atmosphere of a DA or a hydrogen atmosphere WD. Both spectroscopic and photometric astronomical observations can be fit to a grid of analogous synthetic quantities which are obtained from the model atmosphere calculations. One of the most fundamental pieces of physics used to construct DA model atmospheres is the line shapes. The line shapes are used to calculate cross sections of bound-bound transitions which are then used to compute opacities and radiative rates. These values come into play when solving the radiative transfer equation governing the propagation of light through the layers of the atmosphere. Ultimately, this yields the final emergent stellar spectrum. The line profiles represent one of the key pieces of constitutive physics that fundamentally dictates our ability to infer masses and temperatures and use them effectively in our interpretations.

Since the first application of spectroscopic fitting to a large sample of DA WD stars by Bergeron et al. (1992), it has become the most widely used technique to determine effective temperatures and surface gravities of these stars. The spectroscopic method involves comparisons of observed spectra to theoretically modeled spectra; the parameters of the model which yield the best fit are taken to be the best estimate of the fundamental parameters of the actual stars. The popularity of this method can be attributed to the fact that characteristics of Hydrogen line profiles are highly sensitive to changes in atmospheric conditions (Schulz & Wegner, 1981). Relative changes in surface gravities and temperatures manifest as variations in the widths of the profiles and are quantifiable to a high degree of precision.

The success of the spectroscopic technique is well established by the myriad high impact results borne from its application to large samples of DA stars. Determinations of the shape of the DA population mass distribution, the boundaries of the ZZ Ceti instability strip, characterizations of the luminosity function, and the evolution and formation rate of DA WDs were all performed using the spectroscopic method (Bergeron et al., 1992; Liebert et al., 2005; Kepler et al., 2007; Gianninas et al., 2006; Eisenstein et al., 2006). Despite the litany of successful applications of this technique, its accuracy is fundamentally constrained by the fidelity of the physics used to construct the model atmospheres. It has become clear in recent years as data quality improves, that the existing physical models are no longer sufficient to faithfully reproduce the observations. A particularly egregious example of this is the

highly discrepant set of masses and temperatures obtained from fitting different lines in the same star (Fuchs, 2017). Perhaps even more concerning is the emergence of a clear systematic offset between temperature and gravity determinations in large scale comparisons between the spectroscopic versus photometric methods. Spectroscopically inferred temperatures are roughly 10% higher and spectroscopic masses are roughly 0.1 $M_{\odot}$ higher than their photometric counterparts (Bergeron et al., 2019; Genest-Beaulieu & Bergeron, 2019). A re-evaluation of the fundamental physical assumptions and models is well justified.

Model atmosphere codes use a grid of broadened Hydrogen line profiles which span the parameter space of possible transitions, temperatures, and electron densities found in WD atmospheres to synthesize emergent spectra. These codes have historically relied on line profiles calculated using the model of Vidal et al. (1970), known as the Unified Theory of line broadening (VCS). VCS unified the impact approximation and relaxation theory and calculated profiles from the cores out to the far wings for the first time in a self-consistent way. A grid of model atmospheres is used to derive fundamental parameters of DA WDs via the spectroscopic and photometric methods.

WD atmospheres are highly ionized and dense enough that pressure broadening dominates the line shapes. While VCS was pioneering work, it has limitations which cause it to fail at high density. Lemke extended the available calculations using the original VCS code to higher transitions, number densities, and temperatures. However, VCS has difficulty converging at

higher number densities and lower temperatures particularly for higher lines. In cases where Lemke (1997) was not able to complete the calculation, they simply copied the profile from the nearest gridpoint where the code did converge. The code used for this work on the other hand, *Xenomorph* employs a different set of approximations which allows it to probe more extreme conditions, and it does converge for the full range of the parameter space.

Tremblay & Bergeron (2009, hereafter TB09) attempted to scaffold the VCS approach with an ad hoc presciption of the Hummer & Mihalas (1988, hereafter HM88) Occupation Probability Formalism to make the calculations more suitable for higher densities. However, it is worth noting that this does not improve the code's ability to converge for the high density, low temperature conditions. The fundamental physical assumptions are unchanged from those of VCS. Adding occupation probability does change the shapes of the profiles, although the biggest change it induces is a dramatic drop in the intensity of the wings. While line-to-line log g and $T_{\rm eff}$ determinations using these profiles are more consistent, the spectroscopic fits to observational data are actually slightly worse (higher χ^2). As mentioned above, recent studies have exhibited indications of inaccuracies in the VCS (1970) theory including systematic discrepancies in mean mass estimates obtained using different mass determination techniques (Bergeron et al., 2019; Genest-Beaulieu & Bergeron, 2019) and highly discrepant inferred mass and temperature obtained from fits to individual lines (Fuchs, 2017). This suggests there is still a need for further improvement in the line profile calculations.

Since VCS was first developed, there have been many simulation-based line shape codes developed to benchmark both theory and experiment (Stamm & Voslamber, 1979; Gigosos & Cardenoso, 1987; Stambulchik & Maron, 2006; Gomez et al., 2016). While different codes incorporate different pieces of additional physics, there are three main changes which are intended to generate more accurate line shapes than the VCS Unified Theory. The first is a higher order multipole expansion of the Coulomb interaction between radiator and plasma perturbers compared with the dipole approximation of VCS. This allows for gradients in the electric field across the emitting atom. The second change allows for the expansion of the basis set of atomic states (to computational limitations) which leads to higher order Stark terms. Finally, many simulation codes allow for dynamic ions as opposed to the static ion treatment in VCS. The flexibility afforded by the simulation codes along with the fact that time ordering is inherently incorporated in a chronological time evolution of the plasma motivated us to pursue this approach.

This study will mark the first instance in which simulation-based Hydrogen Balmer line shape calculations are developed for use in WD model atmospheres. This warrants some discussion of the simulation construction required to produce line shapes appropriate for model atmosphere calculations. Chief among the necessary considerations is the noise inherent to simulations. The noise properties are affected by the choice of numerical method used to calculate the line profile from the time-evolved dipole moment operator. Another important consideration is the amount of randomness available to the

simulation. We also incorporated a version of occupation probability into the simulation that is based on the distance to the nearest neighbor ions, and we use it to calculate the effect of the occupation probability formalism of Hummer & Mihalas (1988) and of Fisher & Maron (2002) on the line shapes. To our knowledge, this is the first time occupation probability has been incorporated into a simulation line shape code. Ultimately, it is our hope that this will allow us to parametrize this effect, and to what extent the new features affect the emergent stellar spectra as well as make direct comparisons against current standards used in DA WD model atmospheres and their spectroscopic fits. In this preliminary study, we limit the scope to low principle quantum number lines : Hα, Hβ, and Hγ ($n = 3 \rightarrow 2, 4 \rightarrow 2$, and $5 \rightarrow 2$, respectively). We will investigate higher n lines in the future.

To date, there remains a substantial amount of uncertainty regarding the extent to which changes in the line profiles will manifest in the final emergent stellar spectra. In particular, the magnitude and distance from line center at which changes will begin to affect fundamental parameter determinations have not been carefully investigated or parametrized. While a discussion of all the implications of incorporating these new profiles is outside the scope of this work, we intend to investigate these effects in detail in the future. Here, the focus is restricted to detailing the effects of each of the three new features and two different prescriptions of occupation probability applied in the context of a simulation. Stated in a different way, the goal of this thesis is to detail the changes which emerged from an examination of the myriad factors which

affect Hydrogen Balmer line shapes at the conditions of interest in DA WD atmosphere calculations.

Chapter 2

Simulation Stark Broadened Hydrogen Balmer Line Shapes[1]

2.1 Line Broadening in WD Atmospheres

DA WD atmospheres are made up of a dense plasma of essentially pure Hydrogen. The radial extent of the atmosphere spans a range of number densities and temperatures along a continuous gradient (see Fig. 2.1). To construct synthetic spectra, the atmosphere is modeled as a set of thin, discretely stratified layers, each of which has a constant number density and temperature. The set of layers in aggregate will span the same number densities and temperatures that the actual continuously varying atmosphere does.

Investigating the various depths of formation along a given absorption feature in the emergent stellar spectrum allows us to parametrize the plasma conditions at the layer of the atmosphere in which that portion of the line was formed. Figs. 2.2 and 2.3 show wavelength dependent optical depths $\tau_{\rm ross}$ at

[1] This chapter is based on Cho, P.B. et al 2021, ApJ, (in preparation). The author of this document, Patricia Bo Cho, performed all of the analysis. Some ideas and methods were developed collaboratively with the co-authors.

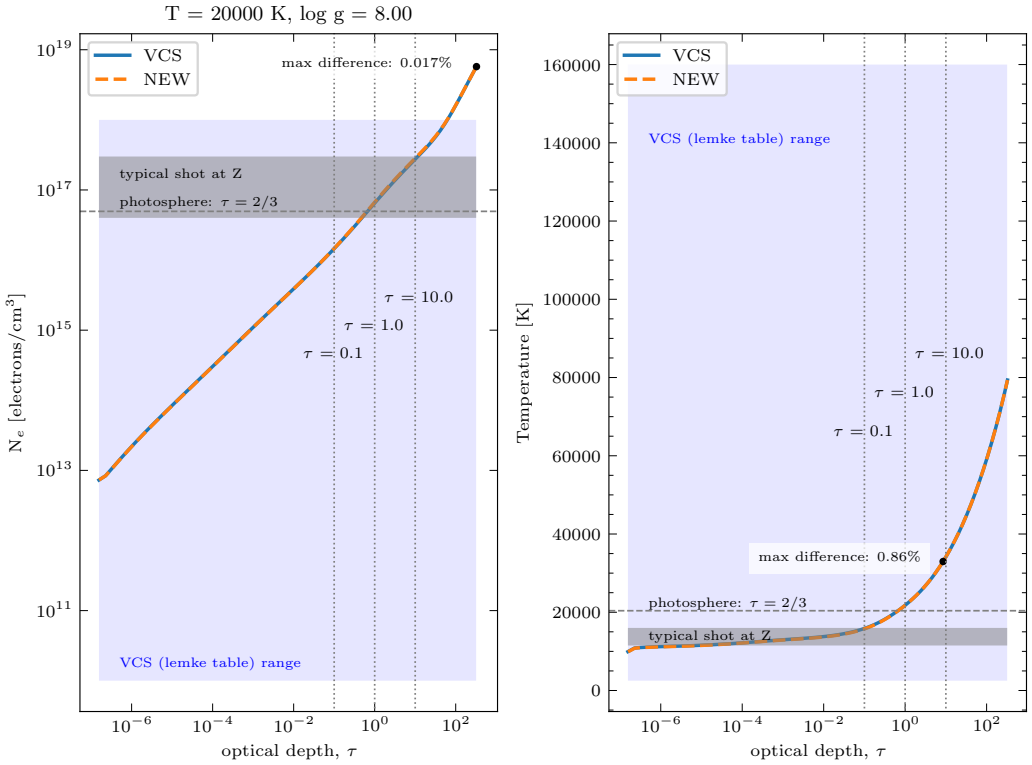

Figure 2.1: Typical DA white dwarf atmospheric structure. Temperature and density profiles are shown as a function of optical depth for a model with T_{eff} = 20,000K and log g = 8. The blue shaded region corresponds to the parameter space covered by the VCS line profiles calculated by Lemke and used to calculate opacities for bound-bound Hydrogen transitions. The vertical dotted lines show conditions at three different optical depths and the horizontal dashed lines point to the conditions at an optical depth of $\tau = 2/3$. The grey shaded region demonstrates the typical range of experimental conditions achievable on the Z-machine. Two different atmosphere models were constructed: one with the VCS line shapes and another with the new Xenomorph profiles containing all of the new features. This ensures the maximum amount of difference between the profiles. The atmospheric structure remains unchanged. The largest difference observed between the two models is less than a percent in the temperature at an optical depth of 10. Therefore, the differences in the profiles are not significant enough to induce a change in the temperature and density profiles of the atmospheres.

which $\tau_\nu = 2/3$. The depth of line formation can vary significantly for different stellar effective temperatures and surface gravities. In particular, the depth of formation of the core of the line is more sensitive to changes in log g and the depth of formation in the wings of the line is more sensitive to changes in effective temperature.

Each set of conditions for each layer of the atmosphere requires a corresponding Hydrogen line shape calculated (or interpolated) at the same conditions to compute the appropriate opacities and perform the radiative transfer. Since the fundamental parameters inferred by the spectroscopic method rely sensitively on the shape of the features in the emergent stellar spectrum, they also rely sensitively on the input Stark-broadened lineshapes. Any inaccuracies in the line shape calculations will propagate through to the mass and temperature determinations.

The primary pressure broadening mechanism at conditions where there is significant ionization is collisions from electrons and ions. These collisions can be approximated by a time-dependent Stark effect. Charged particles induce perturbations in the energy levels of the Hydrogen atoms which correspond to the basis set of stationary state wave functions. The ensemble effect of the close range electric field interactions between the charged plasma perturbers and neutral radiators produces the characteristic Stark broadened line shapes.

The Hamiltonian for a neutral Hydrogen atom (radiator or absorber)

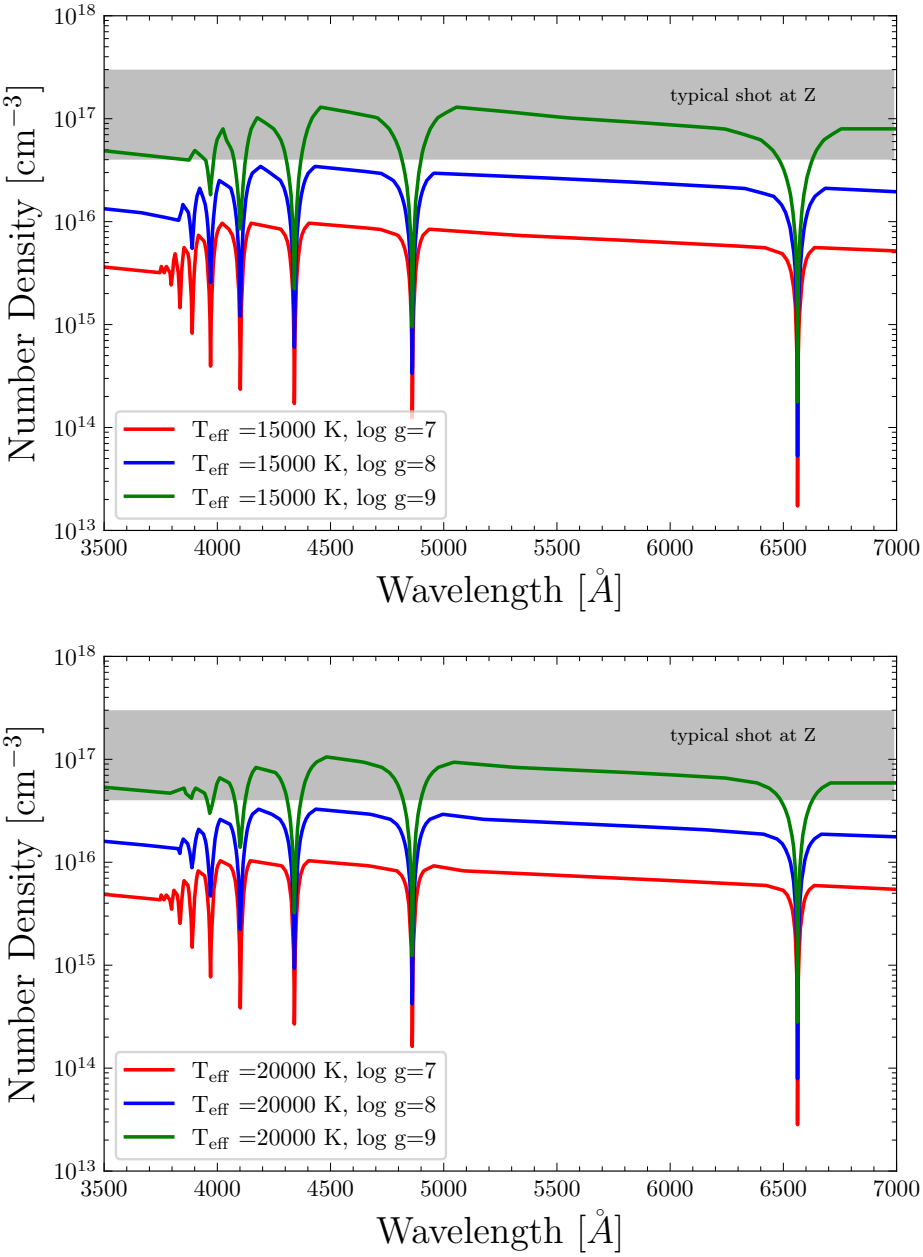

Figure 2.2: Density at depth of formation point for three DA atmosphere models with $T_{\rm eff} = 15,000K$ and $T_{\rm eff} = 20,000K$ for three different values of log g.

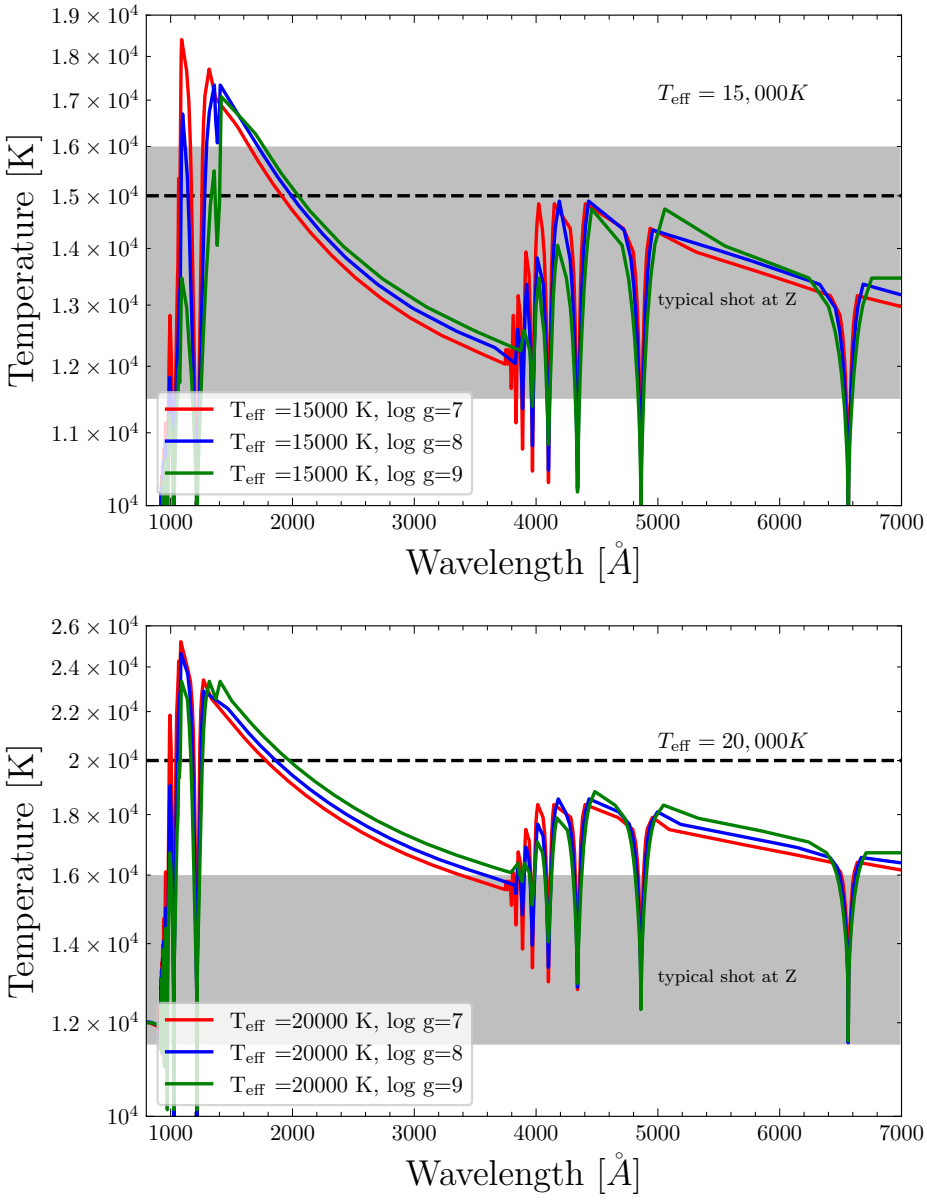

Figure 2.3: Temperature at depth of formation point on extended wavelength range for three DA atmosphere models with $T_{\rm eff} = 15,000K$ and $T_{\rm eff} = 20,000K$ for three different values of log g. The Balmer region of the spectrum is formed higher and at cooler temperatures than the stellar effective temperature.

can be written as

$$H(t) = H_0 + V_{\text{ext}}(\vec{r}, t) \tag{2.1}$$

where we have placed the radiator at $\vec{r}$=0. V is the time-dependent Coulomb interaction between the atom and plasma; this is commonly treated as the net electric field induced by the plasma perturbers at the position of the radiator. In our case, for a pure Hydrogen plasma, the perturbers are simply electrons and protons. H_0 is the unperturbed Hamiltonian of the isolated Hydrogen atom in cgs units:

$$H_0 = -\frac{\hbar^2}{2m}\nabla^2 + \frac{e^2}{|\vec{r}|}. \tag{2.2}$$

The line shapes for spontaneous emission and absorption are assumed to be identical aside from the fact that they are inverted. Though recent laboratory experiments suggest that this assumption may not always hold, we maintain for now the existing convention of calculating emission profiles and taking the inverse to be the absorption profiles.

2.2 Simulation

2.2.1 Plasma Construction and Numerics

Xenomorph (Gomez et al., 2016), the simulation code we use for the line shape calculations, performs a quantum mechanical calculation of the lineshape produced by spontaneous emission from a neutral H atom (radiator) using a time sequence of perturbing electric fields from the evolution of a classical plasma. While some properties, such as electron capture, can only be

captured by a full quantum mechanical treatment of the plasma perturbers, the classical picture is a good approximation for the relevant plasma conditions in white dwarf atmospheres (Gomez et al., 2020; Smith et al., 1969a,b). The code makes use of the Heisenberg picture which evolves the operators in time in contrast with the Schrödinger picture which evolves the wave functions (or state kets). The mechanics involved in the computation of the lineshape (which only requires knowing the time history of the Dipole moment operator) using either the autocorrelation or power spectrum method (discussed in section 2.2.4) make the Heisenberg picture the natural choice.

The dynamics of the system are constructed first. The plasma perturbers are initially placed randomly throughout the spatial extent of a spherical cavity and are assigned velocities taken from a Maxwellian distribution at a given temperature. The perturbers are evolved along straight path trajectories. This is not exactly physically accurate, since inter-particle Coulomb interactions should alter the trajectories. It may be possible for the effects of inter-particle interactions to be sufficiently mimicked using a Debye screened Coulomb potential in lieu of solving the full N-body problem (Stambulchik et al., 2007). The nuances of the choice of screening prescription are discussed in more detail in Section 2.4.

The time history of the evolution of the plasma is then used to calculate the net electric potential ($V(\vec{r}, t)$) produced at the center of the simulation sphere (the position of the radiator). This net electric potential is added to the unperturbed Hamiltonian (H_0) for the isolated Hydrogen atom to construct

the full time-dependent Hamiltonian ($H(t)$). The time dependent Hamiltonian is then used to calculate the time-evolution operator $U(t)$ which is a solution to the time dependent Schrödinger equation:

$$i\hbar\frac{d}{dt}U(t) = H(t)U(t) \tag{2.3}$$

$$U(t_i) = e^{-iH(t_{i-1})\Delta t/\hbar}U(t_{i-1}). \tag{2.4}$$

This time-evolution operator is then used to compute the time-evolution of the dipole moment operator:

$$D_{\alpha\beta}(t_i) = \sum_{\alpha'\beta'} U_{\alpha\alpha'}(t_i)D_{\alpha'\beta'}U^{\dagger}_{\beta'\beta}(t_i) \tag{2.5}$$

where α and β refer to the upper(initial) and lower(final) states of the transition respectively.

Once we have the time sequence of the dipole moment operator in hand, we use the preferred numerical method (autocorrelation or power spectrum) to compute the Stark-broadened line profile (Anderson, 1949; Rosato et al., 2020).

2.2.2 Randomness: Impact Parameter and Maxwellian Velocity Distributions

The artificial conditions of the simulation must be designed to match those of the real physical conditions to the extent possible. The spatial extent of the simulation sphere is dictated by the range at which Coulomb forces are non-negligible and must be set such that the particle count is high enough to

faithfully reproduce the statistical properties of the actual plasma (Stamm & Smith, 1984). Finite bounds to the simulation are also imposed by computational limitations. Throughout the duration of the simulation, some fraction of the perturbing particles will inevitably "leave" the bounds of the simulation and must be reinjected. The reinjection scheme is one of the most delicate pieces of the simulation and must be carefully handled to avoid introducing subtle unphysical behavior. Some of the unanticipated effects can substantially affect the accuracy of the final line shapes.

Regardless of the specifics of the reinjection scheme, the simulation particles must preserve both impact parameter (b) and Maxwellian velocity (v) probability distribution functions. Historically, simulations have preserved these distributions by resampling impact parameter from a limited range of values around the impact parameter the particle was originally assigned and reassigning the same velocity to the particle (Gigosos & Cardenoso, 1987; Stamm & Smith, 1984; Stamm & Voslamber, 1979; Stamm et al., 1984; Djurović et al., 2009). While this approach does properly preserve both distributions, it does so at the expense of the additional randomization afforded by resampling from the full range of possible values. We employ a different approach to reinjection.

Particles with larger impact parameters and larger velocities will leave the sphere more frequently and will therefore need to be reinjected more frequently. If impact parameter and velocity for the reinjected particles are simply resampled from the original theoretical distributions, then these distributions will drift to lower values: the particles will tend to be reinjected along

trajectories that are closer to the central radiator (smaller b) and the simulation plasma will cool (smaller v). We modify the conventional approach by sampling b and v from distributions that have been adjusted by particle lifetime to properly preserve the overall b and v distribution functions. This allows us to maximize randomness in the simulation which improves the noise levels of the line shapes and avoids pathologically unphysical behavior.

We define τ, particle lifetime, as:

$$\tau \propto \frac{\sqrt{1-b^2}}{v} \tag{2.6}$$

We then adjust the probability distribution functions by dividing the original analytical functions by τ. The impact parameter distribution is modified as follows:

$$P_{\text{eq}}(b) = 3b\sqrt{1-b^2} \tag{2.7}$$

$$P_{\text{reinject}}(b) \propto \frac{P_{\text{eq}}(b)}{\tau} = 2b \tag{2.8}$$

The Maxwellian velocity distribution is similarly modified with the thermal velocity defined as the velocity at which the PDF is maximum: $v_{\text{th}} = \sqrt{\frac{2k_bT}{m}}$.

$$P_{\text{eq}}(v) = \frac{4}{\sqrt{\pi}} \frac{v^2}{v_{\text{th}}^3} e^{-v^2/v_{\text{th}}^2} \tag{2.9}$$

$$P_{\text{reinject}}(v) \propto \frac{P_{\text{eq}}(v)}{\tau} = 2\frac{v^3}{v_{\text{th}}^4} e^{v^2/v_{\text{th}}^2} \tag{2.10}$$

Both reinjection distributions have been normalized such that the cumulative probability over the range of possible values sums to 1. Reinjecting the particles using the modified distribution functions properly preserves the

impact parameter and velocity distributions while maximizing the randomness in the simulation (see Fig. 2.4). To our knowledge, this is the first time such a re-injection scheme has been used in simulation-based line profile calculations.

2.2.3 Additional Considerations: Microfield Distribution and Poisson Statistics

It is necessary to verify that the changes to the reinjection scheme have not introduced disruptions to the electric microfield distribution — the distribution of net close-range electric field magnitudes felt by the radiator (Hooper, 1968). The predecessor to the theoretical microfield distributions outlined by Hooper is the Holtsmark distribution (Holtsmark, 1919), which neglected screening effects. We confirm that the Hooper distribution is still properly preserved (see Fig. 2.5).

We also verified that the particle count in a smaller spherical cavity within the larger simulation sphere is Poissonian. Other authors have used a different approach to achieve the proper Poisson statistics — a larger "simulation sphere" feeds particles into a smaller concentric "calculation sphere" with a radius of 3 Debye lengths. Only particles that lie within the bounds of the calculation sphere contribute to the electric field magnitudes Hegerfeldt & Kesting (1988) and Tremblay et al. (2020). While this does save some computation time, the computational expense of the calculation is largely dominated by the integration of the Schrödinger equation, and in particular by the diagonalization of the Hamiltonian. Therefore, we chose to simplify the simulation

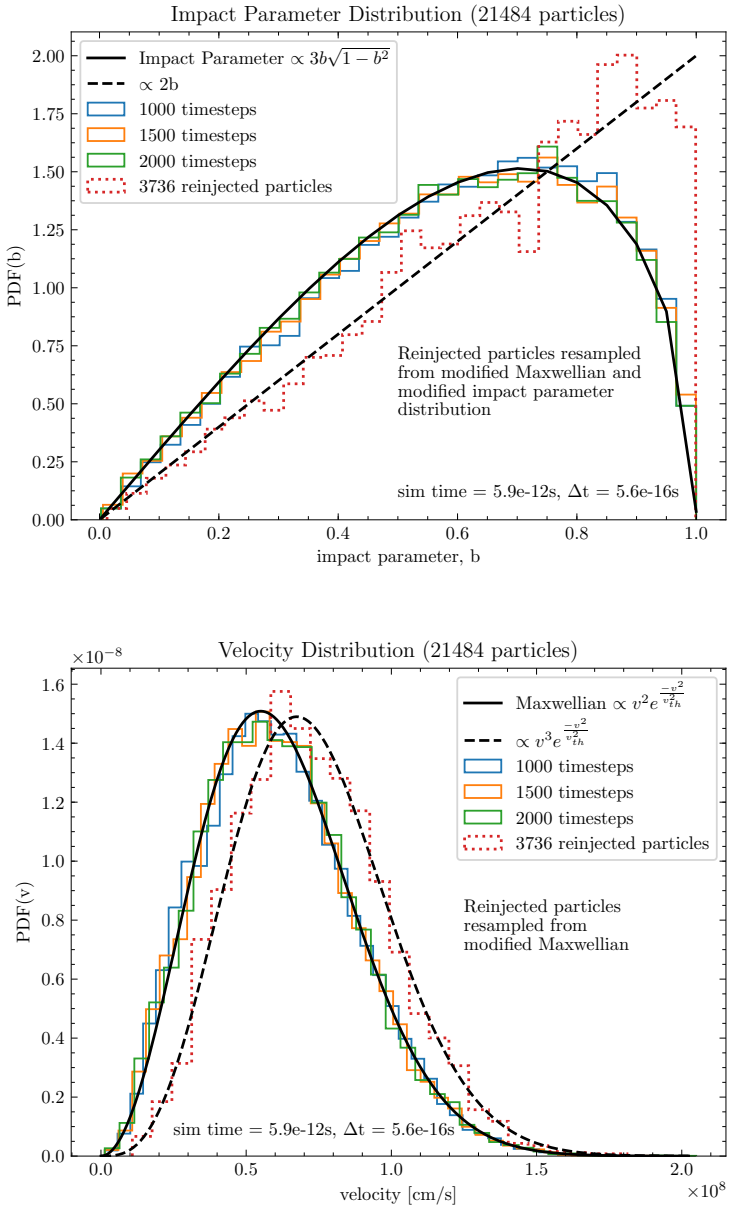

Figure 2.4: Impact parameter and velocity distributions. Both distribution curves are properly preserved when their probability distribution functions are modified by the lifetime for reinjected particles.

construction and specify only a single sphere of 5 Debye radii which is large enough to encompass all particles that make a non-negligible contribution as well as some which will have a negligible effect on the total microfield. Particle counts in *Xenomorph* within a smaller sphere of radius 3 Debye lengths converge to a Poissonian distribution. Contributions from all particles within the simulation sphere are considered.

2.2.4 Debye Screening Effects

To fully mimic physical reality, the simulation code would have to take into account particle-to-particle Coulomb interactions for all of the perturbers in the plasma. Full N-body simulations are still computationally prohibitive. Therefore, most simulation codes instead employ the so-called Debye screened electric potential, given that a minimum of thousands of such simulations would be required to build up the ensemble of electric field time histories that are needed to calculate the averaged profiles. First proposed by the Debye & Hückel (1923) theory, most codes now use Debye screened electric potentials to represent the collective effect of the interparticle interactions. The Debye prescription employs straight line particle trajectories with a modified electric potential. The Debye screening effect is implemented by modifying the electric field from its original Coulombic form (ez_s/r^2):

$$\left|\vec{F}_D\right| = \frac{ez_s}{r^2}\left(1+\frac{r}{\lambda_D}\right)e^{-r/\lambda_D} \tag{2.11}$$

The Debye length, assuming screening from electrons only (λ_D) for a

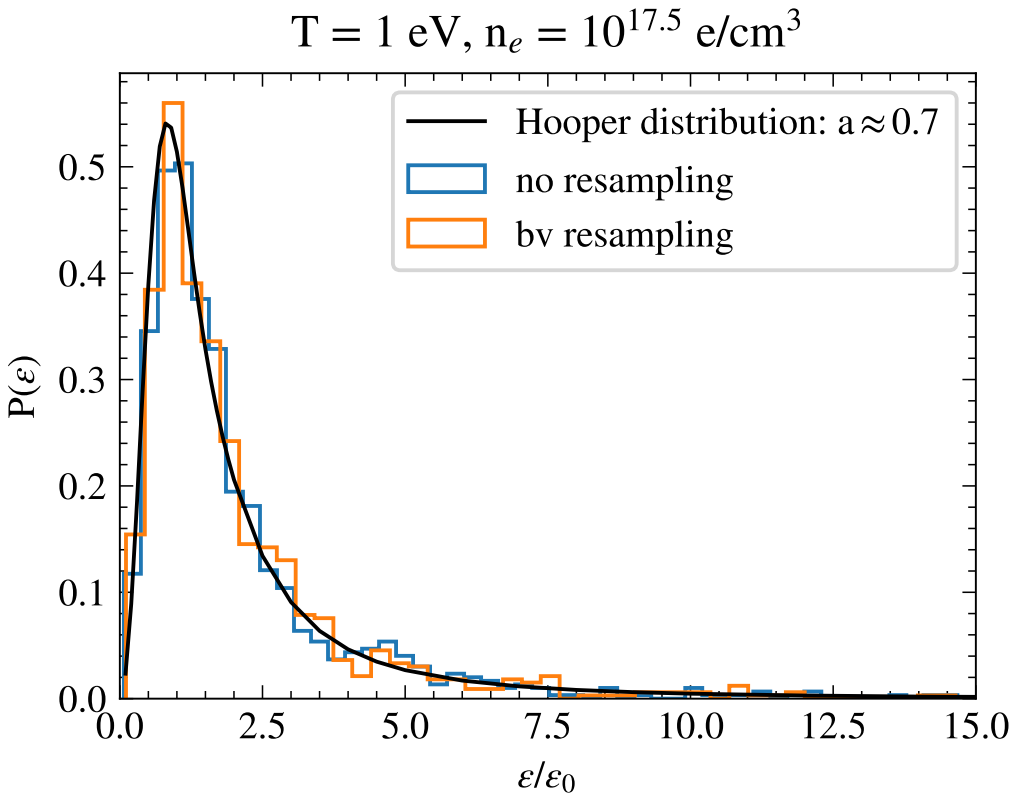

Figure 2.5: Comparisons of microfield distributions. The Hooper microfield distribution is still properly recovered by the new re-injection scheme. Therefore, we can be confident that the new reinjection scheme is properly implemented with regard to its ability to generate the proper microfield distribution.

plasma of temperature T, density N_s, and charge z_s, is given by:

$$\lambda_D = \sqrt{\frac{k_B T}{4\pi N_s e^2 z_s^2}} \tag{2.12}$$

.

The Stark effect will in turn reflect the modified electric potential ($V_D = -z_s \vec{F}_D \cdot \vec{r}_s$) and the line will respond by becoming narrower.

Stambulchik et al. (2007) evaluated the accuracy of the Debye screening formalism using a full N-body simulation which accounts for electrostatic interactions between the plasma particles for a Hydrogen plasma at T=1 eV and $N_e = 10^{18}\text{cm}^{-3}$. They compared the full N-body results to simulation results which employed the Debye screening prescription. The ions were assumed to be screened by both ions and electrons while electrons were screened only by electrons. Thus, $\lambda_{D,i} = \lambda_{D,e}/\sqrt{2}$. They find that the full N-body simulation approach results in less screening, which leads to larger electric field magnitudes than the Debye shielding approach. In the full N-body simulation calculation, the FWHM of the line profile was $\sim$6% greater than that of the screening prescription calculation. This suggests that to properly mimic screening experienced by plasma particles in reality, at least for the particular plasma conditions investigated in that work, the screening may need to be slightly smaller than what is produced by doubly screening electrons. The computational burden of the full N-body simulation prohibits exploring the full plasma parameter space. The Debye screened approach with straight line

trajectories is nevertheless generally taken to be roughly valid at lower densities in the regime of weakly coupled plasmas. The ∼6% difference reported by Stambulchik et al. (2007) suggests this is not an egregious approximation. Additionally, treating the perturbers as classical particles is valid when the average distance between particles far exceeds the thermal de Broglie wavelength (Baranger, 1958b). The conditions of interest in a WD atmosphere satisfy both of these requirements and justifies continued use of Debye screening as a proxy for the full calculations.

For this first generation of line profiles, we chose to adopt the standard approach of singly screened ions and electrons; i.e., both ions and electrons are screened only by electrons, so $\lambda_{D,i} = \lambda_{D,e}$. This likely overestimates the broadness of the line profiles; the singly screened line shape is $\sim 16\%$ broader than the doubly screened one in our calculations. While Stambulchik et al. (2007) report a $\sim 6\%$ difference between their full N-body line shape and their doubly screened line shape, we note that though performed at similar conditions ($T = 1$eV and $n_{\rm e} = 10^{18}$e/cc), their calculations were for Hα. Fig. 2.6 demonstrates qualitatively the differences in broadening resulting from different screening prescriptions. As expected, including screening from more particles results in smaller electric field magnitudes and subsequently, narrower profiles. Nevertheless, our goal of evaluating the effects of the new input physics in the Stark broadening calculations relative to the assumptions made by Vidal et al. (1970) motivated us to use the same Debye screening parameters. It is important to note, however, that the importance of screening should

not be underestimated. Indeed, screening has a larger effect on the line shapes than any of the new physics described in Section 3. Though changes in the cores of the profiles tend to have less of an impact on the final emergent stellar spectra than changes in the wings because the WD spectral features approach saturation due to the purity of atmospheric composition, the effects need to be definitively parameterized by including them in model atmospheres. In future work, we intend to more closely investigate which screening prescription yields the best approximation of physical reality. This may even require a screening approach which varies according to the plasma conditions.

2.2.5 Choice of Numerical Method: Autocorrelation vs. Power Spectrum

Simulation-based line shape codes employ one of two numerical methods to calculate the line shape from the time-evolved dipole moment operator. We will henceforth refer to these as autocorrelation and power spectrum. The power spectrum method described in early texts relies on a recasting of classical electrodynamics and the Poynting theorem into QM analogs (Schiff, 1955). This method treats the electron as a classical oscillator and calculates the resulting Poynting flux propagating out from the current density produced by the oscillating electron. The classical current density ($\vec{J}(r)$) is replaced by its quantum mechanical analog in which the current density is represented by charge density multiplied by velocity. Velocity is then replaced with the momentum operator divided by mass.

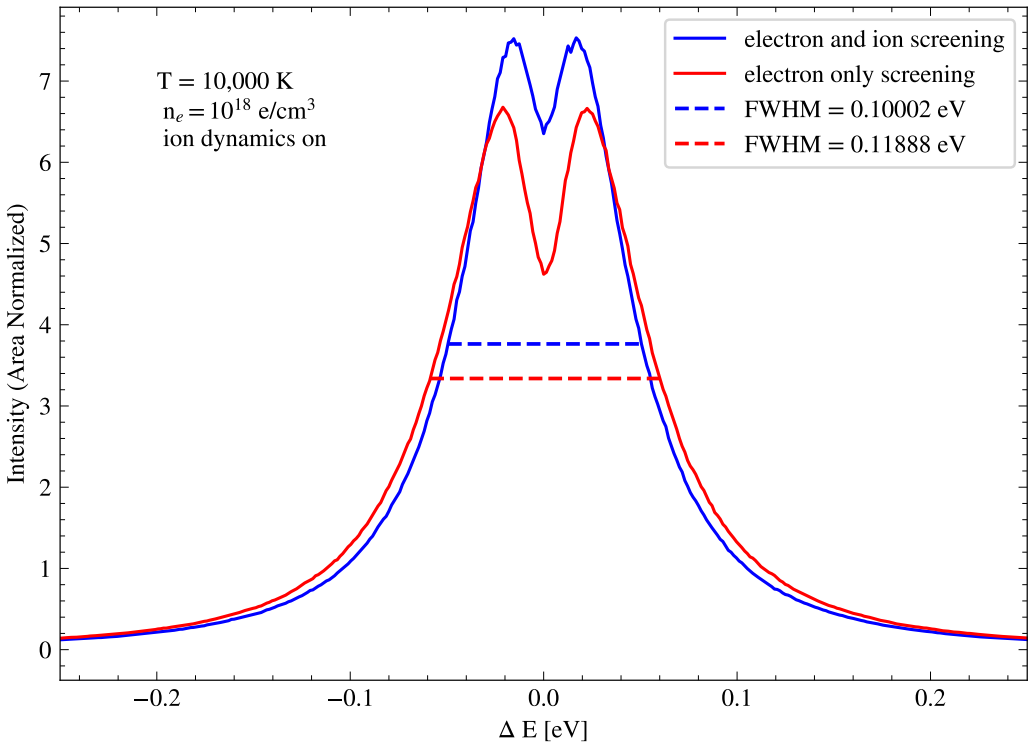

Figure 2.6: The effect of screening on line shape FWHM for Hβ. Increasing the amount of screening experienced by the plasma particles yields narrower lines. Doubly screening ions (in other words, screening ions by both ions and electrons) produces a narrower profile (smaller FWHM) than singly screening both types of particles.

The final expression for the line shape computed using the power spectrum is given by:

$$P(\omega) = \frac{\omega^4}{3\pi\epsilon_0 c^3} \lim_{T\to\infty} \frac{1}{T} \sum_{\alpha\beta} \rho_\alpha \left\langle \left| \int_{-T/2}^{T/2} dt \langle\beta|\vec{d}(t)|\alpha\rangle e^{i\omega t} \right|^2 \right\rangle \tag{2.13}$$

where α and β represent the initial and final states of the transition respectively, and ρ_α corresponds to the density matrix which contains the level populations of the various states considered in the system, the Boltzmann factors. For an isolated line calculation, the density matrix is simply unity. $\vec{d}(t)$ is the dipole moment between the two states and ω is the frequency corresponding to the displacement in energy (ΔE) away from line center.

On the other hand, the dipole autocorrelation method first described by Anderson (1949) and subsequently re-derived using an alternative method by Bloom & Margenau (1953), takes advantage of the properties of Fourier Transforms to recast and simplify the computation. With the autocorrelation method, the characteristic decorrelation of the dipole moment operator reveals the lineshape through the Fourier transform of the dipole moment's autocorrelation function (Baranger, 1958a):

$$P(\omega) = \int_0^\infty dt \sum_{\alpha\beta} \rho_\alpha \vec{D}_{\beta\alpha} \cdot \langle U(t) \vec{D}_{\alpha\beta} U^\dagger(t) \rangle_{\rm av} e^{i\omega t}. \tag{2.14}$$

Here, the capital $\vec{D}$ indicates this is the matrix corresponding to the operator form of the dipole moments. α and β again represent the initial and final states of the transition, and U is the time evolution operator.

Historically, simulation-based line shape codes have chosen to use the dipole autocorrelation function. However, the noise properties of the power spectrum method yield much cleaner final profiles. Though the rate of convergence for both methods is the same and scales as the inverse of the square root of the number of iterations as expected ($1/\sqrt{N}$), the variance of the power spectrum method is much lower (Rosato et al., 2020). Our implementation of the autocorrelation method compared to the power spectrum method corroborates these findings (see Fig. 2.7). We therefore choose to use the power spectrum method; the advantage of this method has been recognized in recent work (Stambulchik et al., 2007; Rosato et al., 2020).

2.2.6 VCS Shortcomings

Critique of the accuracy of VCS goes back to the 1970s, beginning with Lee (1971). Lee (1971) pointed out that VCS unifies the impact limit in the line core with the static (one-electron) limit in the wings, but this unification of the two limits doesn't mean the resulting line shapes are correct across the entire profile. While Lee (1971) has many criticisms of VCS, probably the most important is that the one-electron limit has not been established to produce the correct wing behavior. In reality, the line shape is influenced by the combined effect of ion and electron microfields and particularly as densities increase, simultaneous close approaches of more than one plasma particle become more common. Additionally, Godfrey et al. (1971) pointed out that VCS does not include time-ordering which may cause VCS to underpredict the width, as

demonstrated by Roszman (1975). Since TB09 profiles are calculated using the VCS formalism, these points also apply to the TB09 profiles.

VCS precedes much of the work that led to the set of new physical assumptions incorporated in *Xenomorph* described in Section 2.3. This legacy theory, therefore, also uses static ions, the dipole approximation for the Coulomb interaction, and precludes the ability to use an expanded basis set for the calculations. VCS (and by extension TB09) also suffer from calculational limitations. First, VCS/TB09 cannot include the effect of the neighboring states on the transition of interest. For example, if one is calculating an H-beta line shape ($n = 4 \rightarrow 2$), then the calculation should also include $n = 3$ and $n = 5$; neglecting the adjacent states in this way is known as the no-quenching approximation. The no-quenching approximation is suitable at low densities, but at high densities, as perturbative effects increase, this approximation breaks down. Second, for a given transition, VCS/TB09 fails to converge on a solution on the high-density part of the grid. The upper bound on density decreases with decreasing temperature and increasing quantum number, n. To fill out the grid, Lemke and TB09 simply copy over the profile calculated at the nearest condition for which the calculation did converge. In some cases, the same profile is copied over multiple adjacent gridpoints.

In *Xenomorph*, on the other hand, the calculation is performed by considering the total microfield of both ions and electrons together and does not preclude the possibility that multiple plasma particles can approach the radia-

tor simultaneously. Furthermore, by constructing a chronological history of the time evolution of the electric field, *Xenomorph* integrates the time-dependent Schrodinger equation in a way that implicitly includes time-ordering. Finally, *Xenomorph* does not fail to converge at any set of plasma conditions.

2.3 New Physics

Xenomorph incorporates three new pieces of input physics along with time ordering (which is included by default) that represent improvements over the approximations made by VCS. These are ion dynamics, multipole expansion of the Coulomb interaction potential between radiator and perturbers, and an extended basis set. Each new piece of physics can be turned on independently and studied in isolation to examine their effect on WD atmospheres and their emergent stellar spectra.

We computed line profiles along a grid of number density and temperature for the relevant range of plasma parameters — those spanned by the majority of DA WD atmospheres. Specifically, we calculated Hα, Hβ, and Hγ Balmer line profiles at temperatures of 5,000K, 10,000K, 20,000K, 40,000K, and at electron densities of 10^{15} e/cm^3 $-$ 10^{19} e/cm^3 in steps of 0.5 dex.

2.3.1 Agreement with Previous Theory

We begin by establishing correspondence with the VCS calculations to the extent that this is possible. Under the assumption that the VCS theory has been well vetted over the years and is faithful to the physics that it claims

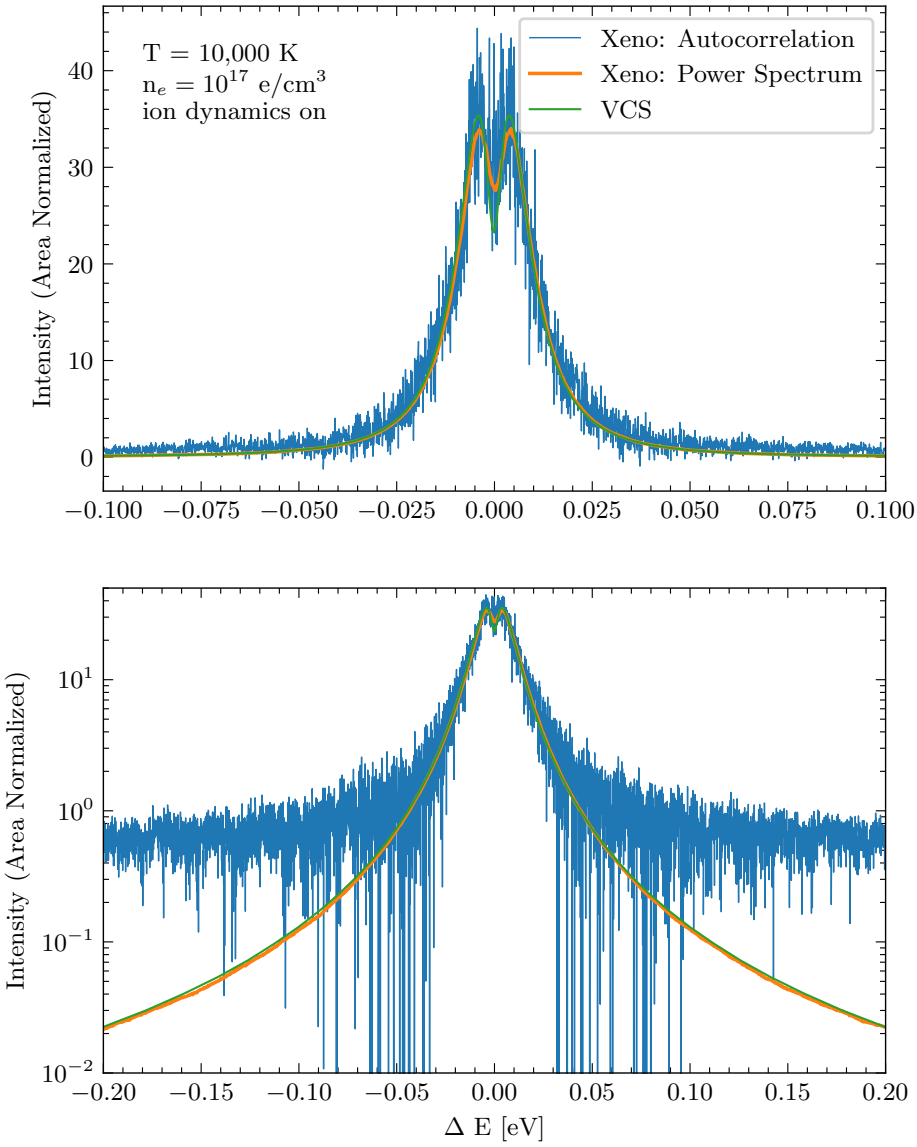

Figure 2.7: Representative Hβ line shape on a linear scale (top) and log scale (bottom). The noise properties of the power spectrum method yield line shapes that are clean enough to use in model atmospheres.

to include, we attempt to reproduce the VCS line profiles using a configuration of *Xenomorph* that is limited to the same physical assumptions. Specifically, we use a configuration of *Xenomorph* that includes static ions, Debye screened plasma perturbers, a set of random configurations of particles and corresponding spatial evolution of those particles which reproduces the Hooper microfield distribution, the dipole approximation for the Coulomb interaction potential, and isolated lines which include only the quantum states of the two principal quantum numbers involved in the transition.

However, there is one fundamental difference between *Xenomorph* and VCS which makes perfect correspondence between the two theories impossible. *Xenomorph* implicitly incorporates the effects of time ordering on the computed line shapes by virtue of the fact that it constructs a time sequence of the electric field history. On the other hand, the standard VCS theory neglects time ordering because it relies on an analytic microfield distribution and does not employ the time-ordering operator. Therefore, we do not expect the central structure of line shape calculations made using the two approaches to agree exactly. As Roszman (1975) points out, the inclusion of time-ordering yields differences in the cores of the line profiles. In particular, including time ordering leads to a lower Hα peak, which is accompanied by an increase in the FWHM. Additionally, time ordering decreases the relative intensity of the Hβ central dip; in other words, the central dip is filled in relative to VCS calculations which neglect time ordering. The slight disagreement observed between the VCS and *Xenomorph* profiles is therefore expected and

the agreement with VCS is otherwise excellent in the wings. To the extent that including time ordering leads to a more physically realistic simulation, we claim that the discrepancies in the core represent another improvement over previous calculations. Figures 2.8, 2.9, and 2.10 show comparisons between the *Xenomorph* and VCS profiles.

2.3.2 Ion Dynamics

The effect of ion dynamics on line shapes has been studied extensively (Gigosos & Cardenoso, 1987; Stambulchik & Maron, 2006; Stamm & Voslamber, 1979). Many of the earliest simulation line shape codes were constructed to examine the effect of moving ions (as opposed to static ions) on the profiles to resolve long standing discrepancies between laboratory measurements and analytical calculations. The inclusion of ion dynamics in the simulation has been shown to yield much better agreement with experimental results in the cores of the profiles. Lineshape calculations used for laboratory diagnostics are particularly concerned with accuracy in this regime. In the context of DA WD model atmospheres however, the lines in the final stellar spectrum are already so broad that changes to the cores have a negligible overall effect.

2.3.3 Multipole Expansion

Inclusion of higher order multipole terms in the Coulomb interaction potential between radiator and plasma perturbers also manifests in the cores of the profiles. Gomez et al. (2016) demonstrated that the Hβ core asymme-

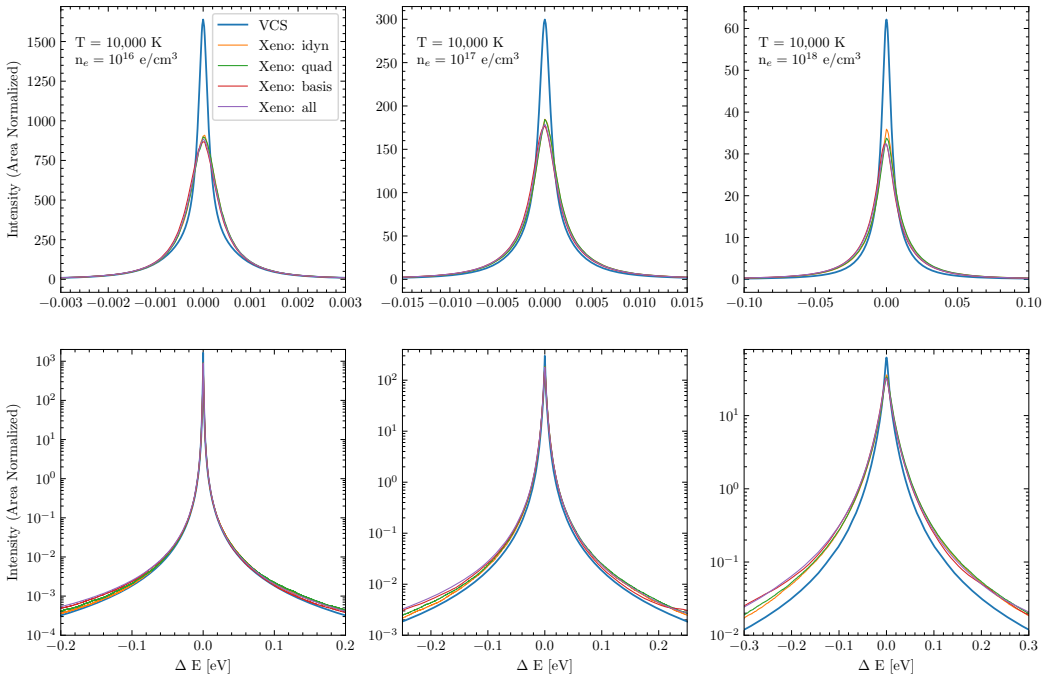

Figure 2.8: Hα calculations with new physics features turned on. Where labeled, each profile includes only one of the additional pieces of input physics. For example, the calculations labeled "Xeno: idyn" use static ions but does not include higher order multipole terms in the Coulomb potential or an expanded basis set. However, all other profiles have been calculated with ion dynamics turned on. For example, the calculations labeled "Xeno: quad" use both static ions and expand the Coulomb interaction potential to include the quadrupole moment but does not use an expanded basis set. This choice follows from the fact that the prolonged presence of a close ion throughout the duration of a given iteration generates large artificial deposits of power in the line profile. This occurs at the frequency corresponding to the disproportionately large and persistent Efield generated by the close ion. Static ions therefore generate spiky profiles in the far wings due to these close ion approaches, and we leave ion dynamics on to avoid this type of pathological behavior in the simulation and in the profiles. Comparisons between VCS and *Xenomorph* exhibit expected disagreement in the height of the cores of the profiles. Inclusion of time ordering in the *Xenomorph* calculations depresses peak height which increases the FWHM. The wings show good agreement between the two theories.

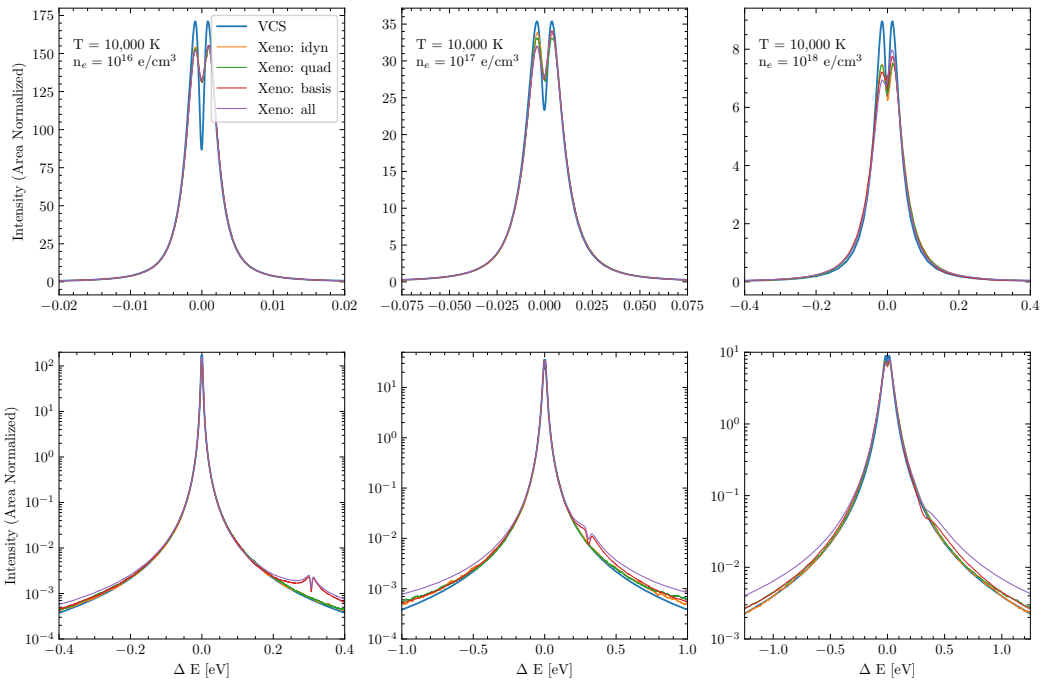

Figure 2.9: Hβ calculations with new physics features turned on. The inclusion of time ordering yields the expected result of decrased relative intensity in the core central dip of the profiles. The wings again show good agreement between the two theories.

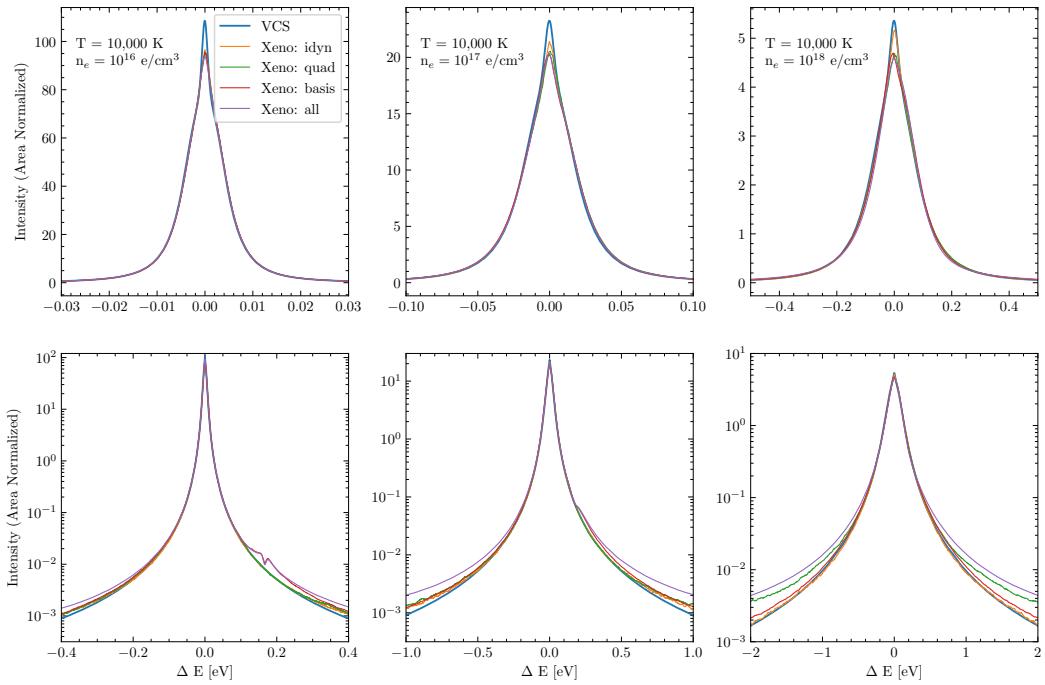

Figure 2.10: Hγ calculations with new physics features turned on. The effects of time ordering are again evident as in the Hα and Hβ calculations, and again we see excellent agreement in the wings of the profiles.

try was much more accurately predicted when the quadrupole term is included in the perturbative potential of the time-dependent Hamiltonian. Closer investigation revealed an error in the calculation of the quadrupole moment in *Xenomorph*. We reproduced Figure 2 of Gomez et al. (2016) with the revised version of the code and find slightly worse agreement with the data. Additional details regarding the difference will be published in an errata. Xenomorph's predictions for the core asymmetry are smaller than measured values. Similar to the changes made to ion dynamics, the inclusion of this feature does not yield large differences in the features of the synthetic stellar spectra.

2.3.4 Expanded Basis Set

The expanded basis set refers to the expansion of the matrix elements of the relevant operators to include those which correspond to neighboring states. In our investigation, we examine the effect of including one additional set of states belonging to the next principle quantum number above the upper level of the transition in question. For example, we include the $n = 4$ states in calculations of Hα — the transition from $n = 3$ to $n = 2$. Expanding the basis set amounts to a more accurate calculation of the Stark effect. In the perturbation theory approach, this equates to including higher order Stark terms in the perturbative expansion.

2.3.5 Occupation Probability

In addition to the broadening of spectral lines through the processes

mentioned in the previous sections, there is another effect in high density plasmas that leads to these lines decreasing in strength and merging with the continuum. This is believed to be the result of the dissolution of atomic states due to the high electric fields of nearby ions, which results in the optical electron being removed from the emitting/absorbing atom. Since this removal occurs for states with negative energies that would otherwise be bound, this effect is often referred to as "ionization potential depression" or "continuum lowering" (Inglis & Teller, 1939). To compute this effect on a particular atomic level, one must average over a statistical ensemble of nearby ions to determine the fraction of atoms that are affected by this process. This results in an "Effective Statistical Weight" or an "occupation probability" for the given state (e.g., Hummer & Mihalas, 1988; Fisher & Maron, 2002). In stellar astronomy, the term "occupation probability" (OP) is most frequently used, and will be used in the remainder of this thesis.

In their most recent work on line profiles, Tremblay & Bergeron (2009) used the Hummer & Mihalas (1988, hereafter HM88) formalism with the implementation of Nayfonov et al. (1999) for calculating the occupation probability of states. This formalism assumes that for each state there is a critical, uniform microfield above which the state no longer exists. Then, using a model for the distribution of the microfield values in the plasma, the fraction of atoms that are experiencing microfields less than this value can be calculated, and this is taken to be the OP for the level. This approach uses the critical microfield as a hard cutoff, and does not consider gradients in this field.

In contrast, Fisher & Maron (2002, hereafter FM02) employ a criterion based on the distance to the nearest ion. They claim this to be more physical since large microfields are almost always produced by nearby ions. They find that a smaller microfield is required to remove an electron since the field becomes stronger in the direction of the ion. Thus, FM02 typically calculate OPs that are smaller than those of HM88. We note that FM02 use a hard cutoff based on the distance to the nearest ion, whereas HM88 use a hard cutoff based on the value of the microfield, assumed to be uniform. In either case, the inclusion of an OP formalism results in lines that are narrower since the broadening effects of the highest microfields are excluded.

This picture of occupation probability is almost certainly too simplistic. The behavior of level dissolution is not binary with survival of the level on one side of the microfield (or nearest-neighbor) cutoff and dissolution on the other side. In addition, while the liberated electron may no longer be bound to a single ion, it may be shared between 2 or more ions in a state with energies and transition probabilities close to their bound state values (Fisher & Maron, 2003). Hence, the spectral features it produces may also not go away suddenly as this criterion is reached.

Nevertheless, the HM88 formalism represents the current state-of-the-art for white dwarf atmospheres, and we employ it and FM02 independently in the calculations that follow. For the implementation of occupation probability in our simulations, we limit the closest approach of the ions such that the total electric field does not exceed the maximum microfield value. To do this,

we cause the closest ion to "bounce" off of an imaginary hard sphere. The simulation doesn't preclude the possibility that two or more ions can make simultaneous close approaches to the radiator. Though these events are less frequent, when they do occur, the ions must be bounced concurrently and at farther distances due to the additional large contribution to the electric field magnitude. For the HM88 prescription, this produces a sharp cutoff in the microfield distribution which qualitatively matches the analytical distribution with a cutoff at β_{crit} used in TB09. For the FM02 prescription, the hard sphere bounce occurs at a radius corresponding to the nearest ion criterion which induces a more severe limitation on large microfields. This produces a microfield distribution which more heavily favors smaller field values.

We have computed grids of line profiles for the same three Balmer lines, Hα, Hβ, and Hγ, on the same temperature and electron density grid with these implementations of occupation probability in addition to all three new pieces of input physics described in the preceding sections.

We have performed a cursory comparison of our profiles which include occupation probability with those of TB09. As expected, The FWHM of the profiles depends on the chosen prescription of occupation probability. The more extreme microfield cutoff energies of FM02 yield narrower profiles than those of TB09 which uses a hard cutoff to the electric microfield energies and which are in turn larger than our implementation of the HM88 prescription which features a rapid but nevertheless continuous decline in the microfield distribution toward higher values. Qualitatively, our profiles differ from those

of VCS in the same way that TB09 profiles do; profiles with occupation probability have narrower cores and sharper drops in the wings.

Additionally, TB09 employ an exponential damping factor to the electron broadening profiles to account for perturbations due to electrons. The physical justification they provide is as follows. Most electron collisions occur so quickly that the electron is unlikely to become unbound. If, on the other hand, the time between successive electron collisions is sufficiently small, the perturbative electric field from the electron can be considered relatively constant and there is a finite probability for the electron to become unbound in accordance with the time-energy uncertainty principle. After a sufficient amount of time, the bound electron will almost certainly undergo ionization if the plasma is in a steady state (Tremblay & Bergeron, 2009). Practically, the correction is applied as follows:

$$\phi'(\nu) = \frac{\phi(\nu)e^{-|\nu-\nu_0|/\nu_c}}{\int_0^\infty \phi(\nu)e^{-|\nu-\nu_0|/\nu_c}d\nu}. \tag{2.15}$$

We applied this damping factor to our own profiles in an attempt to establish correspondence with the profiles of TB09 (see 2.11). Applying the same exponential damping factor described in TB09 results in corresponding wing behavior out to roughly 1 eV from line center for Hβ at 10,000K and 10^{18} e/cc. However, the drop in the wings is much more dramatic in the far wings for the TB09 profiles than allowed by the prescription provided by Eq (15). We will present a more detailed comparison between *Xenomorph* and TB09 profiles in our next publication.

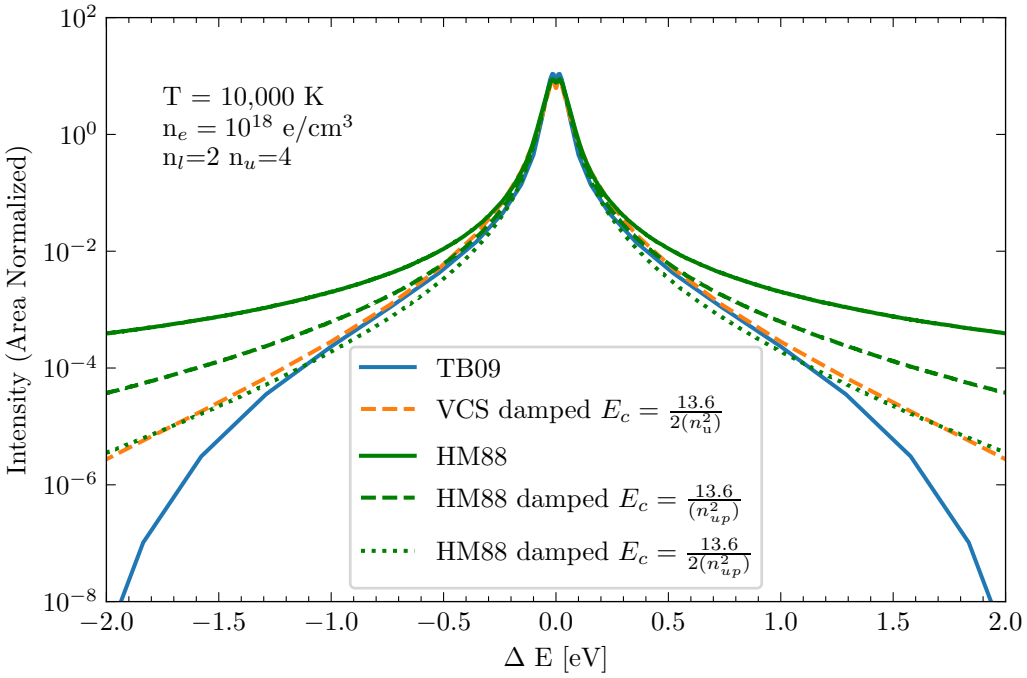

Figure 2.11: Comparison of full line shapes with exponentially damped electron broadening profiles. We apply the wing damping described in TB09 to the VCS profiles as well as to *Xenomorph* calculations performed with the HM88 occupation probability prescription. We achieve decent correspondence TB09 out to about 1 eV if we decrease the rest transition energy in the exponential term by a factor of 2.

2.4 Comparison to Experiment

We adopt the standard mode for validation of theoretical Hydrogen Balmer profiles at high densities by conducting a preliminary and limited comparison of our profiles against the Wiese et al. (1972) experimental data. We use the tabulated TB09 profiles available in the model atmosphere code Tlusty to fit for number density with temperature fixed to the value reported in the TB09 paper. We compare these fits against those performed with our own

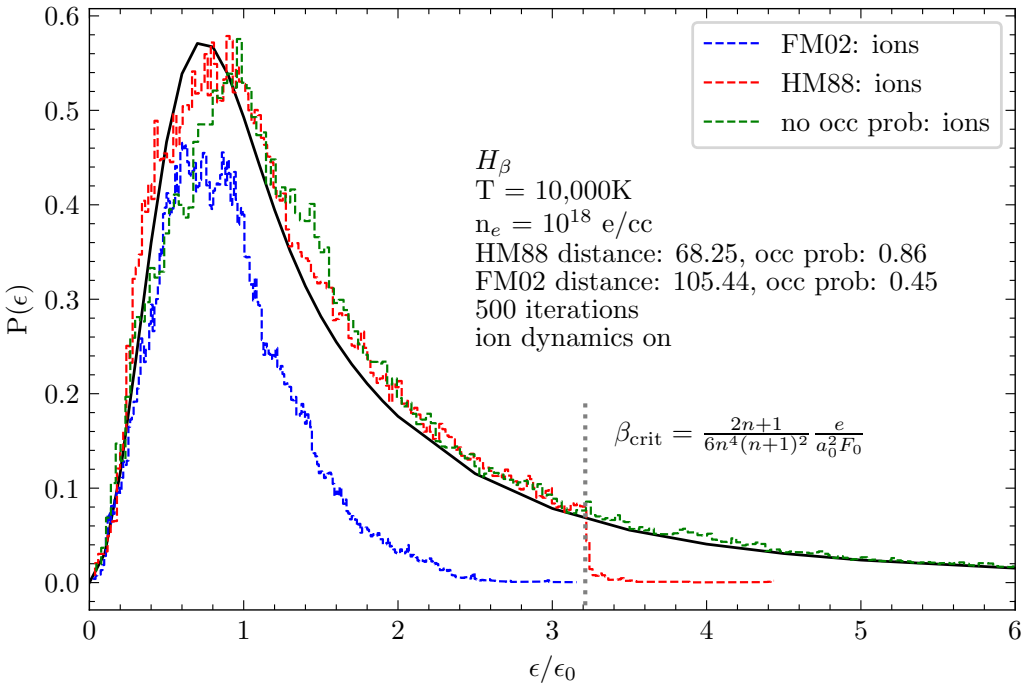

Figure 2.12: Ion and electron microfield distributions compared to Hooper. The ion microfield distribution changes in response to the occupation probability prescription used. Limiting the closest approach of plasma ions and electrons skews the distribution toward smaller electric field values as expected. The vertical dotted line corresponds to the $\beta_{\rm crit}$ value referenced in TB09 — the critical microfield cutoff value. There is very good correspondence between the cutoff in the microfield distribution produced by the HM88 implementation of occupation probability and $\beta_{\rm crit}$.

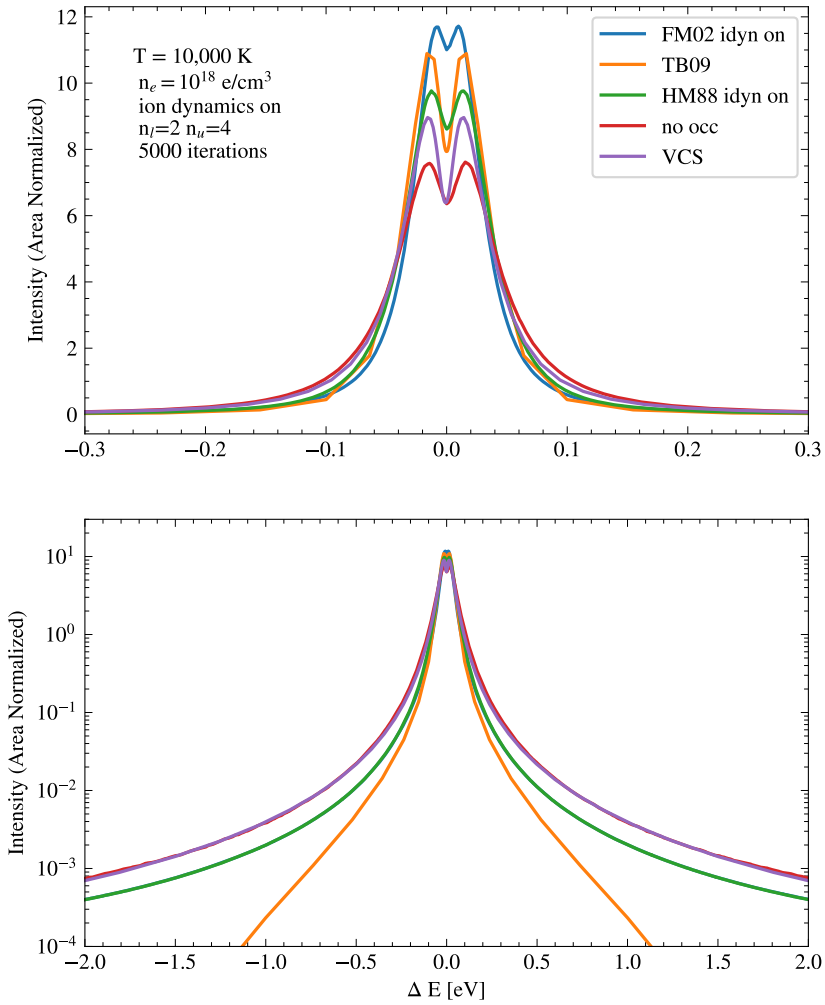

Figure 2.13: Line shape comparison with different occupation probability prescriptions. Incorporating occupation probability results in narrower line shapes. FM02 uses a more severe microfield cutoff compared to HM88. The lower electric field values corresponding to FM02 allows only smaller perturbations and therefore leads to narrower line cores. The wings of the line profiles calculated with FM02 and HM88 are almost identical.

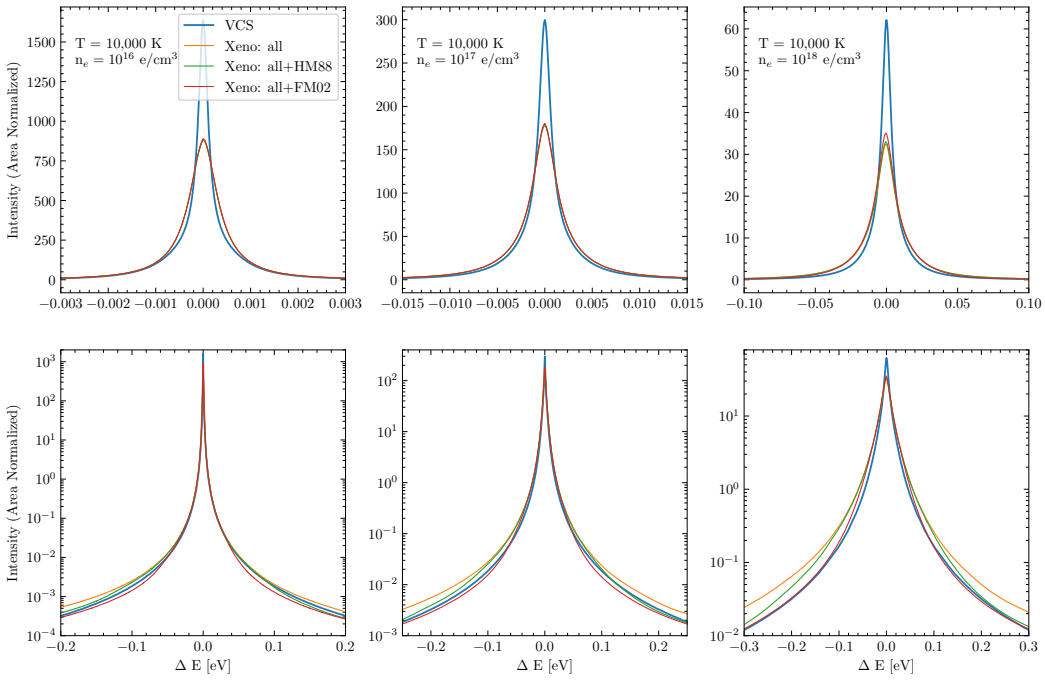

Figure 2.14: Hα calculations comparing different microfield prescriptions.

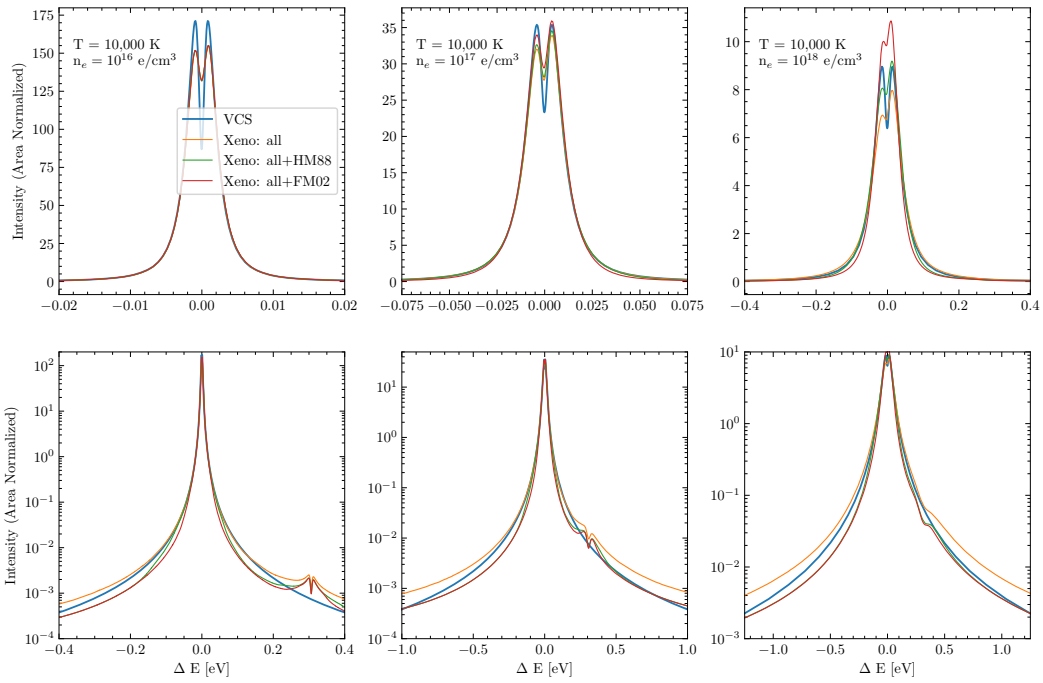

Figure 2.15: Hβ calculations comparing different microfield prescriptions.

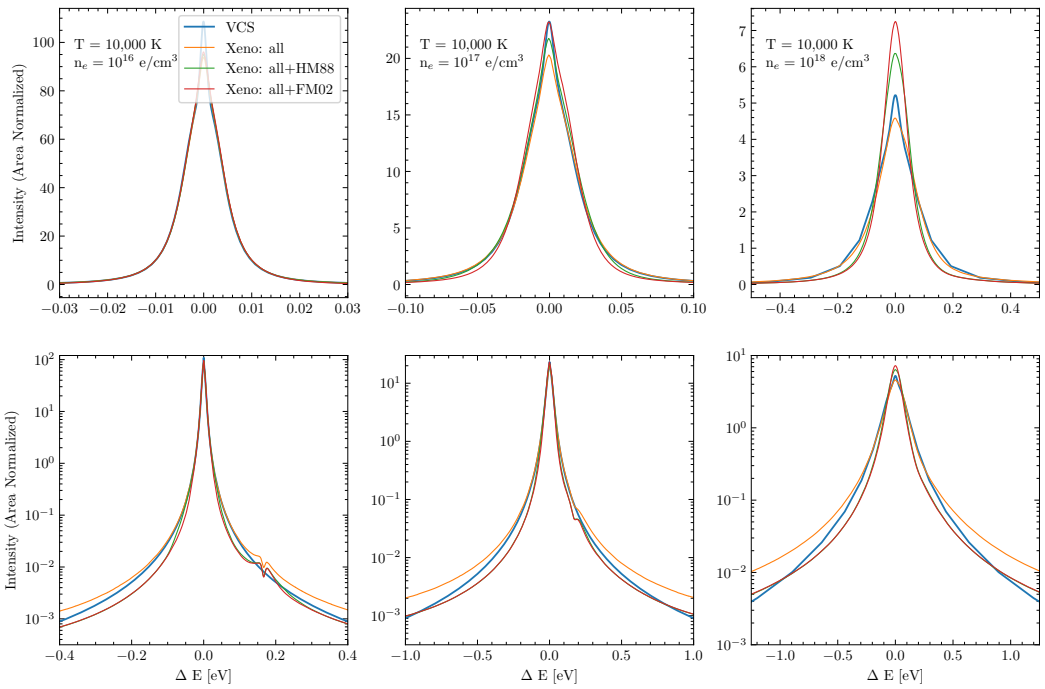

Figure 2.16: Hγ calculations comparing different microfield prescriptions. The effects of time ordering are again evident as in the Hα and Hβ calculations, and again we see excellent agreement in the wings of the profiles.

simulation line profile calculations made with *Xenomorph* (see Fig. 2.1). Appropriate subsections of the Wiese et al. (1972) data which contain a single line were isolated with the left and right cutoff wavelength points corresponding to the points at which the continuum reaches a minimum between the two adjacent lines. The fits were performed using least squares minimization. Electron density, scaling factor, and the continuum polynomial were permitted to float as free parameters. Because the theoretical line profiles are area normalized following convention, we applied a scaling factor to match the intensities of the Wiese data. The continuum in the Wiese data across a given line was fit using a second order polynomial and added to the line profiles to bring the continuum levels into agreement.

Xenomorph shows improvements in the fit to the Wiese data in two regards. First, the Hβ profile fit in the core is vastly improved owing to the combined contribution from all three new pieces of input physics. In particular, ion dynamics and the expanded basis set produce the bulk of the core asymmetry and the improvement in the fit to the data in the core of Hβ. Additionally, the number densities inferred by independent fits to Hβ and Hγ match much more closely between the *Xenomorph* fits. While the number densities inferred using the TB09 profiles differ by $\sim$12% between the two profiles, those inferred using the Xenomorph profiles differ by less than 1%.

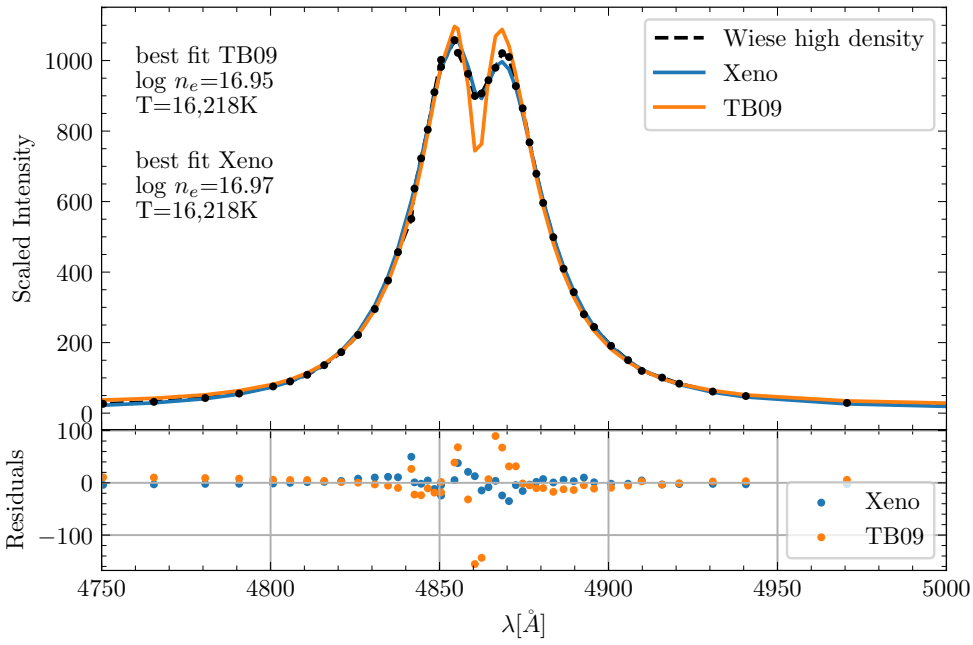

Figure 2.17: Fits to high density Wiese data: Hβ. The core asymmetry is much more accurately predicted by Xenomorph which significantly improves chi-square.

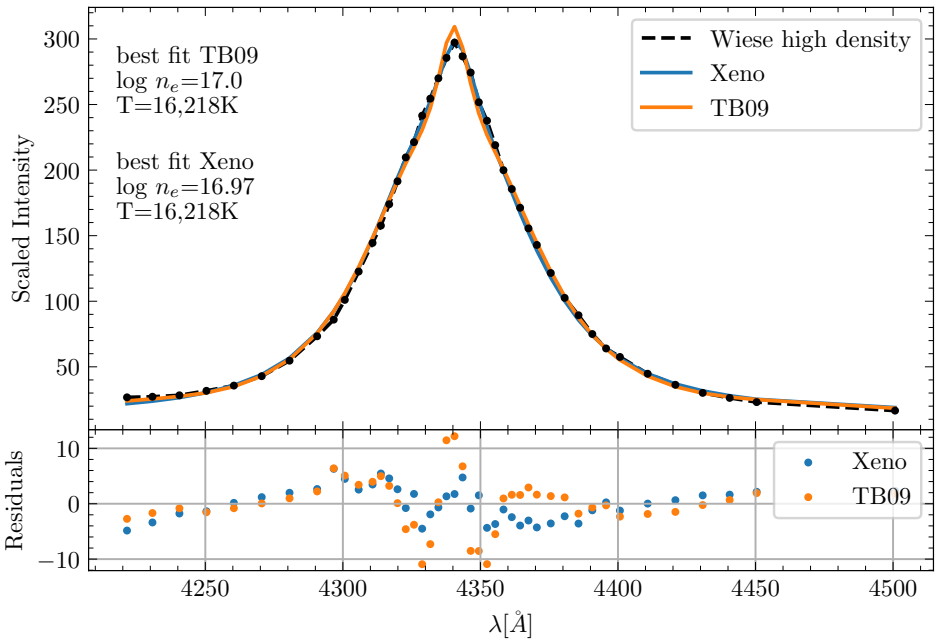

Figure 2.18: Fits to high density Wiese data: Hγ. The best fit number density obtained using *Xenomorph* is almost identical to that obtained for Hβ. On the other hand, the number density obtained using fits to TB09 profiles are roughly 12% higher than that obtained for Hβ.

2.5 Summary

We present new line shape calculations of the first three Balmer spectral lines: Hα, Hβ, and Hγ intended for use in DA WD model atmosphere calculations. The line shapes were calculated using *Xenomorph*, a simulation-based plasma code. We implement a novel approach to reinjection which uses modified distribution functions that take into account the higher probability that particles with large impact parameter and/or velocity will preferentially leave the bounds of the simulation more quickly. This allows us to preserve the

correct impact parameter and velocity distributions throughout the duration of the simulation while maximizing randomness in the simulation.

We found that using a different numerical method than most simulation codes yielded much cleaner line profiles with far better noise properties. We choose to use the power spectrum method employed by Stambulchik & Maron (2006) instead of the autocorrelation method and achieve much cleaner lines, eliminating the possibility of encountering any potential spurious effects when interpolating throughout the grids of profiles for model atmosphere calculations. The cleaner profiles also eliminate the need to perform any smoothing in particularly noisy regions of parameter space or out in the wings of the profiles where noise increases.

Xenomorph incorporates three improvements in the treatment of Stark broadening over previous codes: ion dynamics, inclusion of the quadrupole moment in the Coulomb interactions between radiators and perturbers, and an expanded basis set which includes states from neighboring principle quantum numbers. Additionally, by virtue of the fact that a time history of the electric field is constructed and used to integrate the Schrödinger equation, time-ordering is inherently included in the simulation. *Xenomorph* also has the flexibility to include a simulation-based approach to occupation probability by limiting the closest approach of particles, both to exclude particles within a given radius (FM02) and to limit the maximum value of the electric field (HM88). Two different occupation probability frameworks have been incorporated to study the difference in their effects on the line shapes. These

correspond to the FM02 and the HM88 formalism. The HM88 implementation in our simulation was tuned to produce an electric microfield distribution similar to the analytical distribution implemented by Tremblay & Bergeron (2009).

We constructed four separate grids of line profiles corresponding to each of the three new pieces of input physics and one grid which simultaneously incorporates all of the new features. We also performed two set of calculations with all new features turned on in addition to the HM88 and FM02 occupation probability formalism. Ion dynamics and quadrupole terms in the Coulomb interaction produce minor changes relative to VCS. Calculations performed with an expanded basis set generate small features which mimic the next higher Balmer line in the blue wings of the profiles. These may turn out to produce an appreciable difference in the synthetic stellar emergent spectra. The automatic inclusion of time ordering leads to larger differences than any of the individual pieces of new physics, particularly in the core of Hα.

We also perform initial investigations of the effect of two different permutations of the Debye screening prescription on Hβ. Screening ions by both ions and electrons and electrons by electrons yields a FWHM for Hβ that is $\sim$15% smaller than screening both ions and electrons only by electrons. The choice of screening prescription has the potential to induce larger changes in the final emergent stellar spectra than any of the three new pieces of input physics described above. Similarly, the effect of OP outweighs that of any of the new input physics, particularly in the wings of the profiles. The particular

choices made in implementation affect the final calculations and the literature offers more than one possible formalism. Future publications will systematically investigate the different choices for OP implementation and their effects on model atmospheres. We also hope to incorporate comparisons against laboratory data to test these different OP formalisms.

The questions and topics investigated in this thesis have long been debated in the atomic physics community. Many of them remain open sources of debate. We present this collection of topics in the context of a simulation code developed specifically for the relevant parameter space of DA WD model atmospheres, though the range of possible calculations extends somewhat beyond this. Many of the topics reviewed in this publication require further extensive examination and their implementation in *Xenomorph* and other line profile codes will benefit from further refinement, in particular, OP. Despite the remaining outstanding questions, the combination of all of the new physics and time ordering in the line shape calculations produces significant improvements in fits to laboratory data, and in particular to the standard for the Hydrogen Balmer series: the Wiese et al. (1972) data. Though we will continue to investigate occupation probability and refine our implementation, we intend to tabulate grids of line profiles for use in DA WD model atmosphere calculations and for comparison against existing standards for line profiles. These databases will be provided in a forthcoming publication.

Chapter 3

Outlook

Theoretical advancements within the atomic physics community can experience some delay in propagating over to astronomy. Often, there is significant overlap in the relevant parameter space of interest, however, the applications and contexts are different. The theory of Stark broadening in Hydrogen Balmer line shapes is a prime example. Line shape calculation techniques have experienced significant advancements since the emergence of the VCS calculations presented in the early 1970s. However, aside from an ad hoc prescription of occupation probability, white dwarf model atmosphere calculations have relied on the original VCS theory, and the atomic physics advancements have yet to be incorporated into the astrophysical models. Additionally, computational limitations which prohibited the use of simulations for Stark broadened line shapes five decades ago are no longer prohibitive. This thesis represents significant progress toward incorporating the physical theoretical advancements as well as numerical advantages of a simulation based Stark broadening code in Hydrogen Balmer line shapes for DA WD model atmosphere calculations.

The initial iteration of the code, *Xenomorph*, was first developed several years ago, and incorporated the three new pieces of input physics de-

scribed in the previous chapter. This thesis presents a series of improvements in two regards. Improvements in the numerical scheme used to perform the calculation, now make large grids of calculations tractable, where previously, synthetic noise levels and long computation times limited the use case to single one-off calculations. Secondly, the simulation construction scheme required a number of modifications to eliminate unphysical behavior and artificial periodicities in the electric field distributions and particle spatial distributions. The changes also increase the randomness available to the simulation which brings the plasma closer in line with physical reality. This thesis also performs preliminary investigations of different Debye screening and occupation probability prescriptions applied in a simulation context including an ad hoc exponential damping factor applied to the profiles. The final comparisons to the standard Wiese data suggest that the additional physics produces improved profiles which improve the fidelity of the fits.

There are multiple threads we intend to follow up in future work. Shortly following the publication of the details of the modifications, we intend to perform production runs to generate full grids of profiles tabulated for use in model atmosphere calculations. These grids will be provided in a subsequent publication and immediately be made available to the community for validation and further study. We also plan to incorporate the profiles into the stellar model atmosphere code Tlusty in order to perform a systematic investigation of the effects of the profiles on fundamental parameter determinations of effective temperature and surface gravity. We intend to follow the

initial explorations of occupation probability and screening prescription with a more detailed and robust investigation. We will attempt to identify improvements to the formalism, originally developed in the context of equation of state calculations, to make them more suitable for line shape calculations.

In aggregate, the changes made to the code as well as the investigations detailed here represent a long overdue interrogation of the physical assumptions which the white dwarf community has relied on for the past five decades. In some cases, for example, the incorporation of higher order Coulomb terms, the improved approximations may not have large implications for the final fundamental parameter determinations of the stars themselves. In others, for example, the inclusion of ion dynamics, the addition may have implications only for certain lines. In still others, like the screening prescription and the details of our implementation of occupation probability, the changes may have larger systematic effects on the ensemble statistics of the larger population of white dwarf stars. The work presented in this thesis therefore, represents the beginning of an exciting series of advancements which are important to bring our theoretical models in line with the level of precision which the past decades' improvements in instrumentation have brought to observational data.

Bibliography

Anderson P. W., 1949, Physical Review, 76, 647

Baranger M., 1958a, Phys. Rev., 111, 494

Baranger M., 1958b, Phys. Rev., 112, 855

Bergeron P., Saffer R. A., Liebert J., 1992, ApJ, 394, 228

Bergeron P., Dufour P., Fontaine G., Coutu S., Blouin S., Genest-Beaulieu C., Bédard A., Rolland B., 2019, ApJ, 876, 67

Bloom S., Margenau H., 1953, Phys. Rev., 90, 791

Debye P., Hückel E., 1923, Phys. Z, 24, 185

Djurović S., Ćirišan M., Demura A. V., Demchenko G. V., Nikolić D., Gigosos M. A., González M. , 2009, Phys. Rev. E, 79, 046402

Eisenstein D. J., et al., 2006, ApJS, 167, 40

Fisher D. V., Maron Y., 2002, European Physical Journal D, 18, 93

Fisher D. V., Maron Y., 2003, , 81, 147

Fontaine G., Brassard P., Bergeron P., 2001, PASP, 113, 409

Fuchs J. T., 2017, PhD thesis, The University of North Carolina at Chapel Hill

Genest-Beaulieu C., Bergeron P., 2019, ApJ, 871, 169

Gianninas A., Bergeron P., Fontaine G., 2006, AJ, 132, 831

Gigosos M. A., Cardenoso V., 1987, J. Phys. B: At. Mol. Phys., 20, 6005

Godfrey J. T., Vidal C. R., Smith E. W., Cooper J., 1971, Phys. Rev. A, 3, 1543

Gomez T. A., Nagayama T., Kilcrease D. P., Montgomery M. H., Winget D. E., 2016, Phys. Rev. A, 94, 022501

Gomez T. A., et al., 2020, Phys. Rev. Lett., 124, 055003

Hegerfeldt G. C., Kesting V., 1988, Phys. Rev. A, 37, 1488

Holtsmark J., 1919, Annalen der Physik, 363, 577

Hooper C. F., 1968, Phys. Rev., 165, 215

Hummer D. G., Mihalas D., 1988, ApJ, 331, 794

Inglis D. R., Teller E., 1939, ApJ, 90, 439

Kepler S. O., Kleinman S. J., Nitta A., Koester D., Castanheira B. G., Giovannini O., Costa A. F. M., Althaus L., 2007, MNRAS, 375, 1315

Lee R., 1971, Journal of Physics B Atomic Molecular Physics, 4, 1640

Lemke M., 1997, A&AS, 122, 285

Liebert J., Bergeron P., Holberg J. B., 2005, ApJS, 156, 47

Marigo P., 2001, A&A, 370, 194

Narayan G., et al., 2019, ApJS, 241, 20

Nayfonov A., Däppen W., Hummer D. G., Mihalas D., 1999, ApJ, 526, 451

Rosato J., Marandet Y., Stamm R., 2020, Journal of Quantitative Spectroscopy and Radiative Transfer, 249, 107002

Roszman L. J., 1975, Phys. Rev. Lett., 34, 785

Schiff L., 1955, Quantum Mechanics

Schulz H., Wegner G., 1981, A&A, 94, 272

Smith E. W., Vidal C. R., Cooper J., 1969a, J Res Natl Bur Stand A Phys Chem, 73A, 389

Smith E. W., Vidal C. R., Cooper J., 1969b, J Res Natl Bur Stand A Phys Chem, 73A, 405

Stambulchik E., Maron Y., 2006, Journal of Quantitative Spectroscopy and Radiative Transfer, 99, 730

Stambulchik E., Fisher D., Maron Y., Griem H., Alexiou S., 2007, High Energy Density Physics, 3, 272

Stamm R., Smith E. W., 1984, Phys. Rev. A, 30, 450

Stamm R., Voslamber D., 1979, Journal of Quantitative Spectroscopy and Radiative Transfer, 22, 599

Stamm R., Botzanowski Y., Kaftandjian V. P., Talin B., Smith E. W., 1984, Phys. Rev. Lett., 52, 2217

Tremblay P.-E., Bergeron P., 2009, ApJ, 696, 1755

Tremblay P., Beauchamp A., Bergeron P., 2020, ApJ, 901, 104

Van Horn H. M., 2015, Unlocking the Secrets of White Dwarf Stars, doi:10.1007/978-3-319-09369-7.

Vidal C. R., Cooper J., Smith E. W., 1970, , 10, 1011

Wiese W. L., Kelleher D. E., Paquette D. R., 1972, Phys. Rev. A, 6, 1132

Winget D. E., Hansen C. J., Liebert J., van Horn H. M., Fontaine G., Nather R. E., Kepler S. O., Lamb D. Q., 1987, ApJLett, 315, L77

Vita

Patricia Bo Cho was born in Long Beach, California. She graduated cum laude with a Bachelor of Arts in Asian Studies with a focus on Linguistics from Williams College in 2010. After a brief stint at a high school in Boston, followed by one in the private sector, followed by a meandering tour through various farms in the Pacific Northwest, she returned to school. She attended Columbia University in New York where she completed the Astrophysics major. She then matriculated into graduate school at the University of Texas at Austin to study astronomy. She was awarded the DOE NNSA Laboratory Residency Graduate research fellowship in 2020.

Email address: patricia.cho@utexas.edu

This thesis was typeset with LaTeX[†] by the author.

[†]LaTeX is a document preparation system developed by Leslie Lamport as a special version of Donald Knuth's TeX Program.